Earth and Planetary Science Letters 606 (2023) 118050

Contents lists available at ScienceDirect

Earth and Planetary Science Letters

journal homepage: www.elsevier.com/locate/epsl

Basin formation, magmatism, and exhumation document southward migrating flat-slab subduction in the central Andes

Joel E. Saylor [a,*], Kurt E. Sundell [b], Nicholas D. Perez [c], Jeffrey B. Hensley [d], Payton McCain [c], Brook Runyon [e], Paola Alvarez [f], José Cárdenas [g], Whitney P. Usnayo [g], Carlos S. Valer [g]

[a] Department of Earth, Ocean and Atmospheric Sciences, University of British Columbia, Vancouver, BC, Canada
[b] Department of Geosciences, Idaho State University, Pocatello, ID, USA
[c] Department of Geology & Geophysics, Texas A&M University, College Station, TX, USA
[d] Department of Earth and Atmospheric Sciences, University of Houston, Houston, TX, USA
[e] Department of Geosciences, University of Arizona, Tucson, AZ, USA
[f] Universidad Mayor de San Andrés, La Paz, Bolivia
[g] Universidad Nacional San Antonio Abad del Cusco, Cusco, Peru

ARTICLE INFO

Article history:
Received 18 October 2022
Received in revised form 5 January 2023
Accepted 8 February 2023
Available online xxxx
Editor: A. Webb

Keywords:
detrital zircon
maximum depositional age
sediment provenance
U-Pb geochronology
chronostratigraphy

ABSTRACT

The Central Andean Plateau is the largest plateau formed in a non-collisional setting and is taller, wider, has thicker crust, and has greater retroarc shortening than any other region of the modern Andes. It also hosts some of the thickest Cenozoic strata in the Andes, which were deposited synchronously with punctuated widening and narrowing of the magmatic arc. Multiple hypotheses have been advanced to explain these unique characteristics, yet the detailed, plateau-scale Cenozoic basin history needed to test these hypotheses remains unavailable and therefore has not been integrated into the established records of deformation and magmatism. Here we synthesize new detrital zircon maximum depositional ages (MDAs) and sediment provenance analysis of non-marine strata from ~15°–16.5°S with existing records of sediment accumulation, deformation, and magmatism from ~14°–24.5°S to develop a model of the Eocene–early Miocene evolution of the Altiplano-Puna plateau region. Stratigraphic correlations based on the new MDAs show a Paleocene–Eocene unconformity/condensed section followed by resumption of rapid sediment accumulation. Rapid sediment accumulation resumed at 46–43 Ma at 15–16°S, at 36 Ma at 18°S, and as young 19 Ma at ~23°S. Provenance data presented herein indicate that Eastern Cordilleran detritus appeared in Altiplano strata at progressively younger ages to the south. The southward progression of this basin reorganization proceeded in lockstep with initiation of exhumation in the Eastern Cordillera, and also a lull in the magmatic arc followed by widespread volcanic flare-up. We present a model in which the observed stratigraphic hiatus, along with the magmatic lull and flare-up, orogenic widening, and high-magnitude shortening, are upper plate responses to shallowing and resteepening of an late Paleocene–early Miocene flat slab beneath the Altiplano-Puna plateau. In the proposed model initial slab flattening was driven by late Paleocene–early Eocene subduction of buoyant oceanic crust: potentially a Manihiki Plateau Conjugate. Subsequently, southward shallowing and resteepening of a late Eocene–early Miocene flat slab beneath the Altiplano-Puna Plateau was driven by subduction of an asperity on the Nazca Plate which we tentatively identify with the Juan Fernandez Ridge. The geographic coincidence of all of these features suggests that the flat slab hydrated and weakened the upper plate lithosphere, thereby facilitating later development of the suite of unique features which characterize the Central Andean Plateau.

1. Introduction

The central Andes serves as an archetype for the geodynamic processes active in cordilleran systems. Its geologic history is used to develop diagnostic criteria to identify geodynamic processes and predictive models which form interpretive paradigms for global

* Corresponding author.
E-mail addresses: jsaylor@eoas.ubc.ca (J.E. Saylor), kurtsundell@isu.edu (K.E. Sundell), ndperez@tamu.edu (N.D. Perez), jeffreybhensley@gmail.com (J.B. Hensley), pmccain5877@gmail.com (P. McCain), brookrunyon@gmail.com (B. Runyon), pp_aazz@hotmail.com (P. Alvarez), cardenasroque@gmail.com (J. Cárdenas), whitpao14_95@hotmail.com (W.P. Usnayo), casulvaler@gmail.com (C.S. Valer).

https://doi.org/10.1016/j.epsl.2023.118050

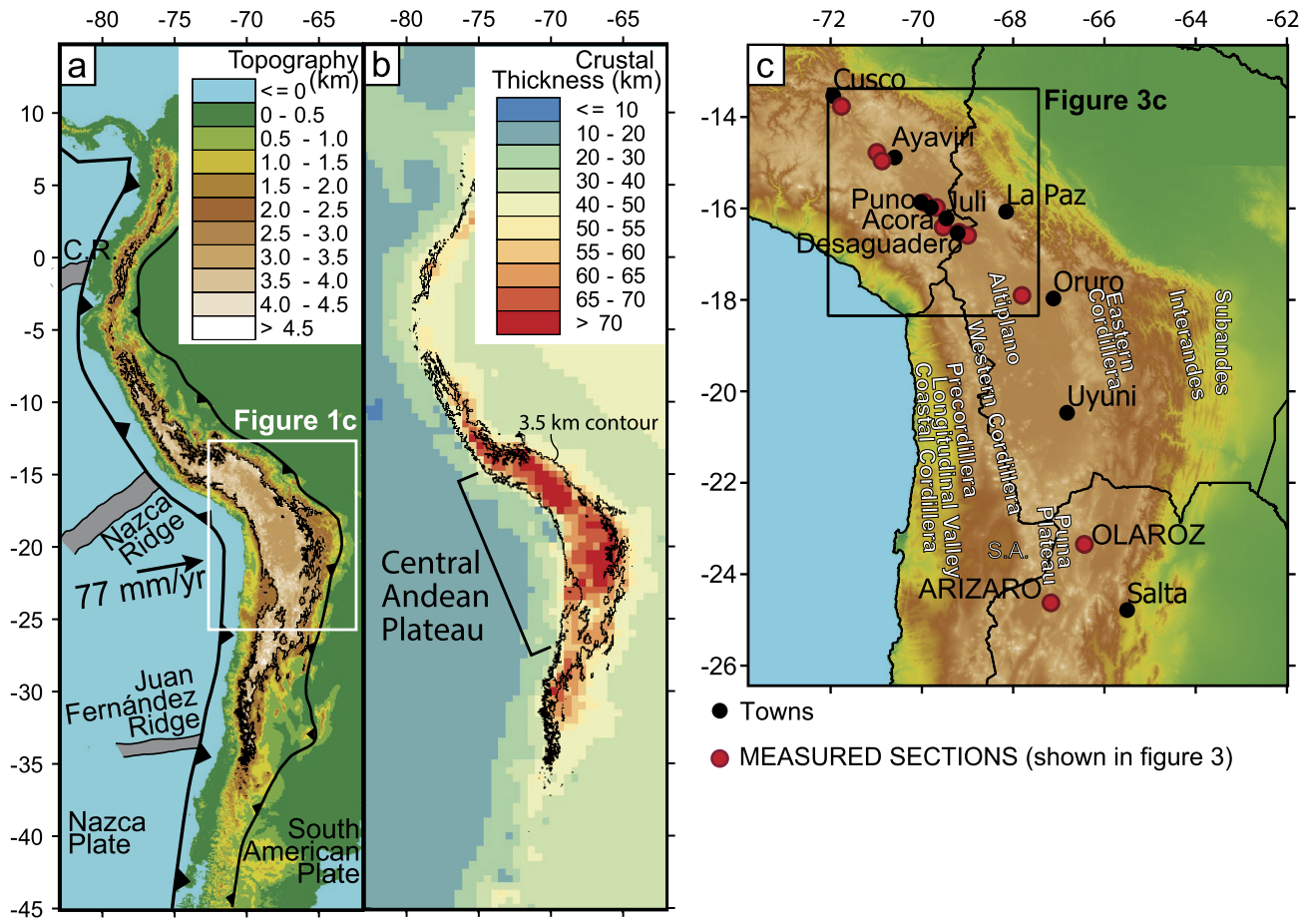

Fig. 1. (A) Digital elevation model showing the anomalous height and width of the Central Andean Plateau (CAP, after Horton, 2018a). (B) Crustal thickness map highlighting the extreme thicknesses beneath the CAP (from Rivadeneyra-Vera et al., 2019). (C) Digital elevation model of the Central Andean Plateau showing the locations of stratigraphy shown in Fig. 3. Abbreviations: C.R.: Carnegie Ridge, S.A.: Salar de Atacama.

cordilleran orogenic systems (e.g., DeCelles et al., 2009). Yet uncertainties in the timing and pace of upper plate processes associated with the evolution of the prominent Central Andean Plateau (CAP) hamper development of a generalizable model. For example, flat subduction has been correlated with both surface uplift over the flat slab and dynamic subsidence above the steepening leading edge of the subducted plate (Jadamec et al., 2013; Eakin et al., 2014a; Dávila and Lithgow-Bertelloni, 2015) or subsidence over the flat portion of the subducted plate (Liu et al., 2011; Axen et al., 2018). Discriminating these two scenarios impacts the interpretation of other cordilleran systems where insufficient or excess subsidence is observed.

The central Andes is also an excellent location to test the impact of flat subduction on the upper plate because its geological history includes elements that have been independently correlated with flat subduction. For example, the inboard migration of magmatism followed by a voluminous and widespread volcanic flare-up, typically attributed to flattening and resteepening of the subducted plate in the North American Cordillera (Coney and Reynolds, 1977; Constenius et al., 2003; Copeland et al., 2017), is also seen in southern Peru (Sandeman et al., 1995; Mamani et al., 2010). Similarly, inboard migration of deformation in North America has been attributed to slab flattening (Brown et al., 1988; Bird, 1998; Humphreys, 2009), as it has in Bolivia (Martinod et al., 2020) where deformation migrated from the Western to Eastern cordillera in the Eocene (Rak et al., 2017; Buford-Parks and McQuarrie, 2019). These features serve as independent indicators of flat subduction and can be used to assess its timing and extent, and correlated to basin records to assess its impact on basin evolution.

The CAP is also an anomaly in the Andes and its anomalous characteristics have been explained by models invoking mutually incompatible geodynamic processes. For example, the topographic prominence of the CAP along the >7,000 km length of the Andes has been attributed to both slow and continuous crustal thickening (Barnes and Ehlers, 2009) and removal of dense, overthickened lithosphere (Saylor and Horton, 2014; Garzione et al., 2017; Göğüş et al., 2022). Its anomalous width, with distances from the trench to the eastern deformation front of 600–800 km (Fig. 1A), has been attributed to both upper and lower plate effects (McQuarrie, 2002; Horton et al., 2022, and citations therein). The central Andes from ~16°S–24°S has experienced greater shortening than regions to the north or south (Gotberg et al., 2010; Eichelberger and McQuarrie, 2015) and vertical-axis rotations resulting in oroclinal bending (Roperch et al., 2000, 2006, 2011; Rousse et al., 2005; Arriagada et al., 2006, 2008), but neither effect has a clear causal mechanism. Nevertheless, the CAP also hosts the thickest crust in South America (Fig. 1b, Rivadeneyra-Vera et al., 2019), and shortening magnitudes suggest transfer of crustal material from the Eastern Cordillera to the Altiplano (Eichelberger et al., 2015).

Coupled with the anomalous characteristics described above, the CAP, and in particular the Altiplano, hosts extreme thicknesses of Upper Cretaceous–Paleogene strata (>4–6 km). This stratigraphy has been attributed to multiple geodynamic processes which make specific predictions regarding the location, timing, and pace of deposition and its relationship to regional magmatic or tectonic events. Pre-Oligocene stratigraphy in the Altiplano has been

attributed to an eastward-migrating retroarc foreland basin system (Horton et al., 2001; Horton, 2018a). A retroarc foreland basin setting predicts a decrease in sediment accumulation rate accompanying passage of the forebulge and its increase during deposition in the foredeep depozone (e.g., DeCelles and Horton, 2003). It also predicts that both the decrease and increase in sediment accumulation rate occurred while deformation and exhumation were limited to the Western Cordillera. Alternatively, the Altiplano Basin may have transitioned from a retroarc foreland basin to a hinterland basin accompanying a significant jump in the deformation front from the Western Cordillera to the Eastern Cordillera (McQuarrie et al., 2005; Carrapa and DeCelles, 2014; Rak et al., 2017) or development of an independent orogenic wedge in the Eastern Cordillera (Martinod et al., 2020). Both of these models predict that the tectonic setting of the Altiplano transitioned from a retroarc foreland to a hinterland basin at the time of exhumation of the Eastern Cordillera. In this scenario increases or decreases in sediment accumulation rate may be largely independent of migration of a flexural wave attributable to a foreland basin system and may instead reflect the onset of exhumation in the Eastern Cordillera. Anomalously thick or thin stratigraphic packages in the CAP have also been attributed to oscillation between a neutral or extensional regime and a contractional regime (Rochat et al., 1998), as has been documented in the southern Andes (Horton, 2018a), which predicts an alternation between flexural and fault-driven subsidence. Basin formation in the CAP has also been attributed to lithospheric removal via dripping or delamination (DeCelles et al., 2015b; Garzione et al., 2017; Göğüş et al., 2022), predicting isolated basin formation, with no necessary interconnection between isolated basins. Finally, anomalously thick or thin Altiplano stratigraphy may reflect modulation of subsidence magnitude by flat subduction (Perez and Levine, 2020; Runyon et al., 2021). Dynamic uplift during slab flattening and isostatic uplift during flat subduction predict low or no subsidence in the overriding plate (Dávila and Lithgow-Bertelloni, 2015; Flament et al., 2015; Margirier et al., 2015). On the other hand, mantle circulation in a thinned asthenospheric wedge, dynamic forces associated with slab resteepening, and mantle counterflow at the leading edge of the flat slab all predict enhanced subsidence above or in front of the flat slab (Jadamec et al., 2013; Dávila and Lithgow-Bertelloni, 2015; Axen et al., 2018).

The large scale implicated by many of these mechanisms requires equally large-scale observations. However, detailed basin records, including chronostratigraphic correlations, sediment accumulation rates, and timing of unconformities/condensed sections, needed to test models' predictions and assess the impact of flat subduction on the basin record are unavailable. Paleogene nonmarine clastic strata with only low-precision or no biostratigraphic age constraints, in particular, present two challenges. (1) The nonmarine depositional setting hampers lithostratigraphic correlations over the distances need to identify large-scale tectonic processes. (2) Volcanic beds that would provide datable material to facilitate chronostratigraphic correlations are rare in Paleogene strata.

Herein we test the predictions of geodynamic models and the upper plate response to flat subduction by integrating new detrital zircon U-Pb provenance analysis and maximum depositional ages (MDAs) for Upper Cretaceous and Paleogene strata in Peru and Bolivia with published basin records into a transect spanning >10° latitude (14°S to 24.5°S). The data show a Paleocene–middle Eocene unconformity followed by rapid sediment accumulation at ~15°S. The termination of the unconformity and resumption of rapid sediment accumulation post-date the onset of exhumation in the Eastern Cordillera at the same latitude. In addition, the termination of the unconformity, exhumation in the Eastern Cordillera, and magmatic flare-up all become younger to the south at the same rate. We conclude that this pattern is best explained by progressive southward slab shallowing, culminating in local flat slab subduction, followed by its progressive southward resteepening. Our discussion focuses on describing how this model accounts for many of the anomalous characteristics of the CAP described above.

2. Geological setting

Convergence and subduction of the Nazca Plate beneath the South American Plate began in the late Paleozoic (Mamani et al., 2010) and the margin became a well-organized compressional system in the Late Cretaceous (Horton, 2018a). The onset of orogenesis is marked by Late Cretaceous magmatism and exhumation in the Western Cordillera (Vicente, 1990; Mamani et al., 2010), supported by an extensive thermochronological dataset spanning southern Peru–northern Chile showing widespread exhumation starting in the Late Cretaceous (Andriessen and Reutter, 1994; Maksaev and Zentilli, 1999; Schildgen et al., 2007; Wipf et al., 2008; Ruiz et al., 2009; Schildgen et al., 2009b; Gunnell et al., 2010; Juez-Larré et al., 2010; Reiners et al., 2015; Avdievitch et al., 2018; Henriquez et al., 2019). Coeval with the onset of Andean orogenesis, deposition in the Altiplano region transitioned from marine to non-marine during Late Cretaceous–Paleocene retroarc foreland basin evolution (Sempere, 1995).

Exhumation in the Eastern Cordillera progressed from north to south. Exhumation in southern Peru was ongoing between 56 and 31 Ma based on zircon (U-Th/He) and apatite fission track (AFT) ages (Kontak et al., 1990; Perez and Levine, 2020). Biotite Ar^{40}/Ar^{39} and zircon fission track data indicates exhumation in northern Bolivia was ongoing by 48–45 Ma (Benjamin et al., 1987; Gillis et al., 2006), but thermokinematic modelling pushes the initiation to as early as 55 Ma (Rak et al., 2017; Buford-Parks and McQuarrie, 2019). Eastern Cordilleran exhumation in south/central Bolivia was ongoing by 42–40 Ma based on AFT ages coupled with HeFTy modelling (Scheuber et al., 2006; Ege et al., 2007; Eichelberger et al., 2013). In the Eastern Cordillera east of the Puna Plateau exhumation AFT ages indicate a minor Eocene episode of exhumation followed by major exhumation beginning at 28–26 Ma (Deeken et al., 2006; Carrapa et al., 2014). *AFTsolve* and age-elevation models suggest that exhumation began at ~23 Ma (Deeken et al., 2006; Carrapa et al., 2014).

The central Andes from ~16°S–24°S has experienced greater shortening than regions to the north or south (Gotberg et al., 2010; Eichelberger and McQuarrie, 2015). Correspondingly, the region north of ~18–20°S experienced Paleogene counterclockwise vertical-axis rotation whereas the zone to the south is characterized by clockwise rotation (Roperch et al., 2000, 2006, 2011; Rousse et al., 2005; Arriagada et al., 2006). Overlapping in age with these events, the locus of magmatism widened, coeval with a lull or shut-down in magmatism in the Western Cordillera between the Eocene (Mamani et al., 2010) and the Oligocene (Trumbull et al., 2006). Multiple researchers have attributed the shut-down in arc magmatism and migration of magmatism to an Eocene–Oligocene period of shallow or flat subduction in southern Peru and northern Bolivia (Sandeman et al., 1995; James and Sacks, 1999; O'Driscoll et al., 2012; Ramos, 2018). A separate episode of flat-slab subduction has been proposed for northern Chile and Bolivia in the Oligocene–Miocene (Jiménez et al., 2009; Kay and Coira, 2009; Beck et al., 2014; Ramos, 2018).

3. Methods

3.1. Samples and U-Pb analyses

Forty-two samples were collected in the context of newly measured or published stratigraphic sections (Fig. 2). Zircons were

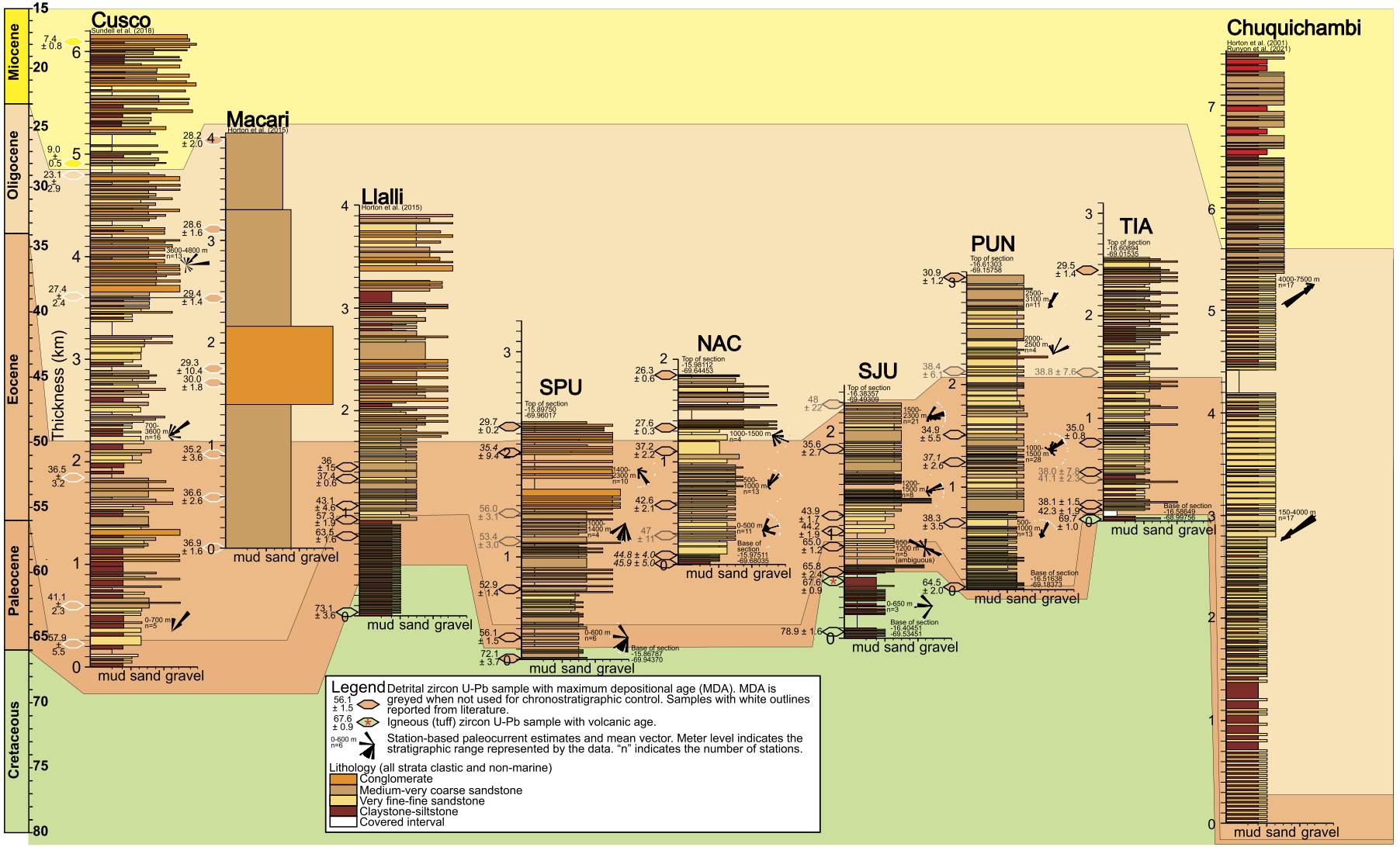

Fig. 2. Regional stratigraphic correlation, showing simplified lithologies at each location and the stratigraphic context of zircon U-Pb samples. Paleocurrent data available in Supplemental Tables 12–14.

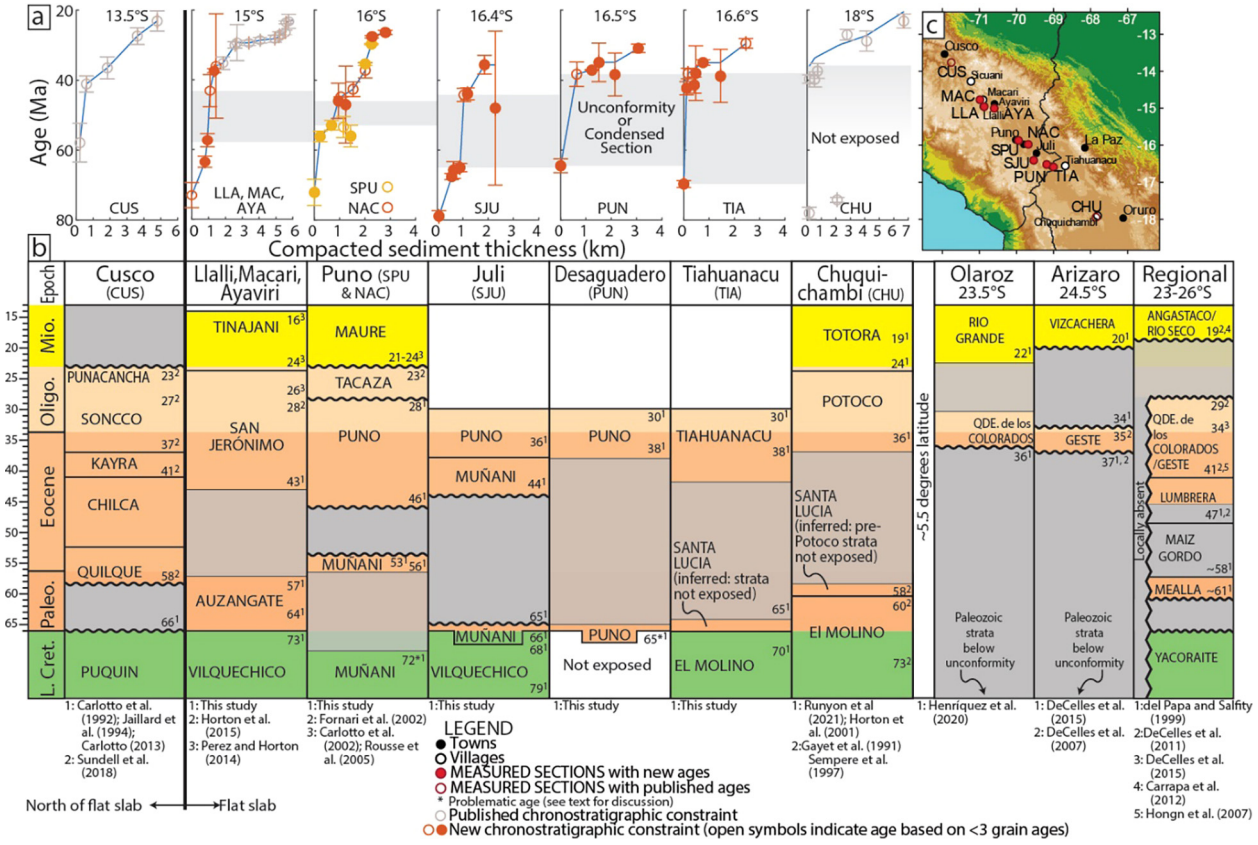

Fig. 3. A) Sediment accumulation records and B) chronostratigraphic diagram both show the regional unconformity and its southward younging. C) Regional map showing the locations of stratigraphic sections with new chronostratigraphic data. Chronological constraints used in panel B are from this study and Gayet et al. (1991), Carlotto et al. (1992, 2002), Jaillard et al. (1994), Sempere et al. (1997), del Papa and Salfity (1999), Horton et al. (2001, 2015), Fornari et al. (2002), Rousse et al. (2005), DeCelles et al. (2007, 2011, 2015a,b), Hongn et al. (2007), Carrapa et al. (2012), Carlotto (2013), Perez and Horton (2014), Sundell et al. (2018), Henríquez et al. (2020), and Runyon et al. (2021).

separated using standard density and magnetic separation techniques. U-Pb analyses were conducted at the University of Houston and University of British Columbia. At the University of Houston, a PhotonMachines Analyte 193 nm ArF laser and a Varian 810 single-collector quadrupole ICP-MS were used, with data reduced by a MATLAB-based code in *UPbToolbox* (Sundell, 2017). At the University of British Columbia analysis was conducted using a Resonetics RESOlution M-50-LR equipped with a UV excimer laser source (Coherent COMPex Pro 110, 193 nm, pulse width of 4 ns) and data was reduced using Iolite 3.4 extension for Igor Pro™.

3.2. Maximum depositional ages

MDAs were determined using three methods: the Youngest Statistical Population (Coutts et al., 2019), the Maximum Likelihood Age (Vermeesch, 2021), and the mean and standard deviation of a Gaussian curve fit to the youngest Probability Density Plot (PDP) age mode (Supplemental Data Table 1). For the latter, the Gaussian curve was fit to the portion of the PDP that included the youngest inflection point. With the exception of one case (see section 4.1 below), if there was discordance among the methods we chose the age yielded by two of the three methods.

3.3. Quantitative provenance analysis

Following the methods laid out by Smith et al. (2023, accepted), we conducted non-negative matrix factorization (i.e., inverse modelling) of Late Cretaceous–Cenozoic U-Pb age distributions from across the Altiplano, including those from Cusco (Fig. 1c, Sundell et al., 2018), the samples presented in this work, and Chuquichambi (Fig. 3c, Runyon et al., 2021) using *DZnmf2D* (Saylor and Sundell, 2021) (Supplemental Table 2). To avoid volcanic zircons which would be geographically non-diagnostic due to airborne broadcasting, only ages >200 Ma were included in the provenance analysis described below. Samples consist of univariate (U-Pb ages only) distributions and were input as kernel density estimates (KDE) with a fixed 20 Myr bandwidth. Prior to factorization, 14 of the samples were merged into seven sample groups to avoid samples with <150 analyses. Each of these seven groups consistent of two merged samples. Samples were merged only with stratigraphically adjacent samples and only samples that were similar were merged into a single group. We factorized to a range of ranks from 2–30, yielding an optimum rank of nine (Supplemental Figure S1). We then compared the factorized distributions for rank nine to empirical potential sources, yielding close fits between most of the factorized distributions and empirical sources. We used those empirical potential sources in a forward Monte Carlo mixing model (*DZmix*, Sundell and Saylor, 2017) to determine the proportions of each empirical source that contributed to the mixed Late Cretaceous–Cenozoic samples.

4. Results

We present 13,171 new U-Pb ages from six stratigraphic sections (Fig. 2 and Supplemental Data Tables 3–8). Zircon ages were used to determine MDAs and quantify sediment provenance for the Late Cretaceous–Paleogene strata. Probability density plots, KDE age distributions, and concordia plots for individual samples are presented in the Supplemental Materials.

4.1. Maximum depositional ages

MDAs are broadly consistent with previously assigned stratigraphic ages but improve precision, allowing investigation of sediment accumulation rates at higher resolution than previously possible. A full comparison between previous radiometric and biostratigraphic ages and MDAs from this study is presented in the Supplemental Material.

For the majority of the forty-two samples the three methods of calculating MDAs yielded ages that were within uncertainty of each other. Most (34 of 42) samples show an upsection younging in zircon MDA (Fig. 2). However, two samples posed particular difficulties. For the lowermost sample at Desaguadero (1PUN002, PUN section) MDAs based on the Youngest Statistical Population and youngest PDP peak yield latest Paleocene–earliest Eocene ages (54.4–57.5 Ma). However, the Maximum Likelihood Age is earliest Paleocene (64.5 Ma), which is consistent with regional trends which indicate uppermost Cretaceous or lowermost Paleocene strata below a regional unconformity encompassing the Paleocene–early Eocene. In light of the regional trends, we opt for the 64.5 Ma age in this case. In the second case, the youngest single zircon grain was not included in the analysis of the sample at Puno (140816-03, SPU section) because it had a non-uniform analysis spectrum and was >16 Myr younger than the next oldest zircon grain. The non-uniform analysis spectrum is attributed to inclusions in the zircon grain which may yield an inaccurate young age.

MDAs define convex-up sediment accumulation curves with a period of slow sediment accumulation (undecompacted sediment accumulation rate ≤0.03 mm/yr) in the Paleogene followed by rapid sediment accumulation in the late Paleogene–Neogene (Fig. 3a). The age of the resumption of rapid sediment accumulation decreases systematically to the south, from ca. 46–43 Ma in the northernmost sections to ca. 36 Ma in the southern Chuquichambi section, consistent with other published records from the southern CAP (Fig. 3b, Sundell et al., 2018).

4.2. Quantitative provenance analysis

Factorized distributions show close matches to eight of 11 empirical potential sources considered here (Fig. 4, Supplemental Table 9). Results of forward mixture modelling using *DZmix* indicate that the proportion of zircon ages attributable to an Eastern Cordilleran source in Cenozoic strata increases upsection for all stratigraphic sections except Cusco (Fig. 5, Supplemental Table 10). Moreover, the age at which the Eastern Cordillera constitutes a significant source systematically decreases to the south.

5. Discussion

5.1. Stratigraphic ages and sediment accumulation

We interpret MDAs as broadly reflective of depositional ages based on the proximity of an active magmatic arc (Mamani et al., 2010), the success enjoyed by previous studies in determining depositional ages using MDAs (e.g., DeCelles et al., 2007; Horton et al., 2015; Sundell et al., 2018; Runyon et al., 2021), the compatibility of MDAs and previous stratigraphic age assignments (see detailed discussion in the Supplemental Materials), and the consistent upsection younging trend shown between most samples. The new MDAs consistently define Paleogene convex-up sediment accumulation curves with an Eocene unconformity or condensed section (accumulation rates ≤0.03 mm/yr) followed by onset of rapid sediment accumulation at locations between 15°S and 18°S (Fig. 3). Combining the new age constraints with published stratigraphic ages shows that the unconformity becomes younger to the south, with a resumption of sediment accumulation between 43 and 46 Ma at 15–16°S but as young as 36 Ma at 18°S and ~20 Ma at 23–24°S (Fig. 6f).

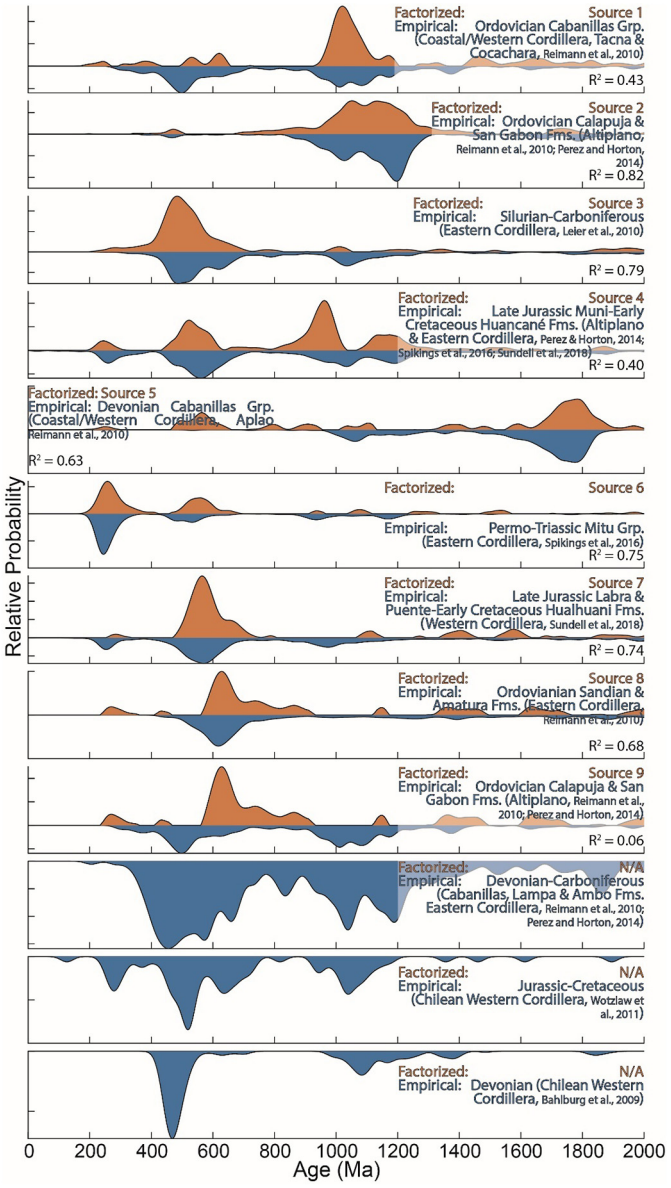

Fig. 4. Comparison between the nine factorized distributions based on non-negative matrix factorization of 50 Late Cretaceous–Cenozoic detrital zircon U-Pb age distributions from this study, Sundell et al. (2018), and Runyon et al. (2021). Factorized distributions were compared to 11 potential empirical sources and the closest matches determined based on cross-correlation of the two distribution sets. Factorized distributions were closest matches to eight empirical distributions whereas three empirical distributions did not match any of the factorized distributions. Distributions are presented as kernel density estimates with 20 Myr bandwidths. Empirical sources from Bahlburg et al. (2009), Leier et al. (2010), Reimann et al. (2010), Wotzlaw et al. (2011), Perez and Horton (2014), Spikings et al. (2016), and Sundell et al. (2018). Data for this figure are in Supplemental Tables 2 and 9.

5.2. Sediment provenance

Mixture modelling of detrital zircon U-Pb age distributions shows several previously undocumented trends. The first is a different upsection trend in sediment derivation between the Cusco section and all sections south of that (Fig. 5). At Cusco there is an upsection increase in Western Cordilleran and Altiplano sources in the Paleogene. This is consistent with predictions for a foreland basin setting (Sundell et al., 2018), where an advancing fold-thrust

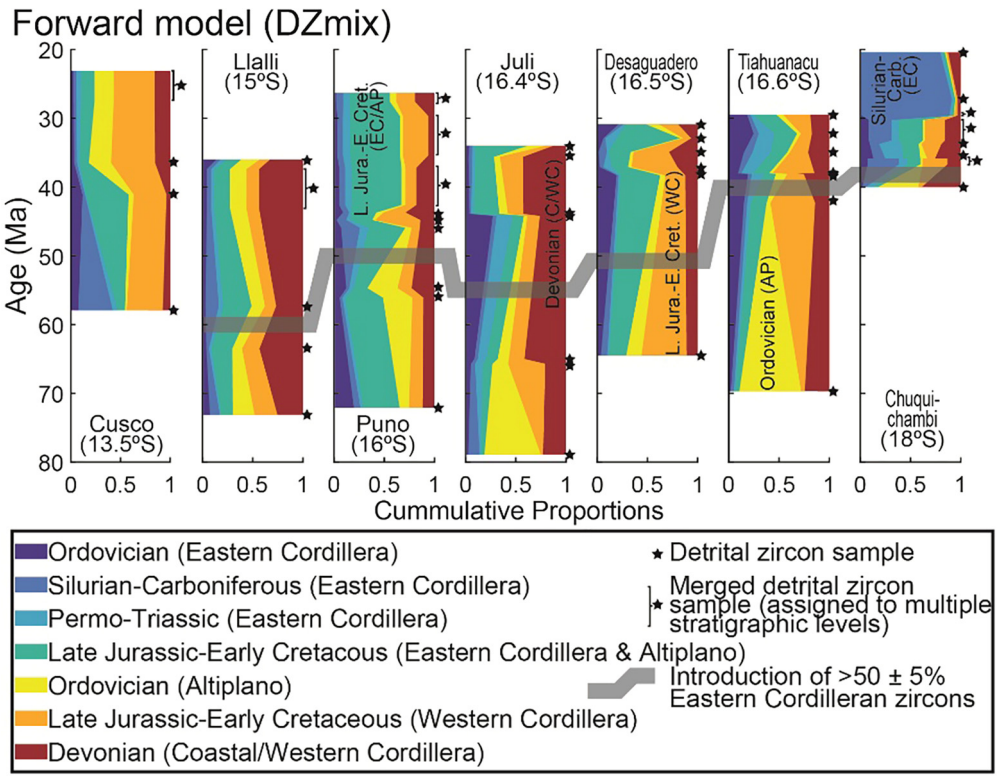

Fig. 5. Results of DZmix modelling of samples from this study, Sundell et al. (2018), and Runyon et al. (2021) using the eight closest matches to the factorized distributions. Whereas at Cusco there is an upsection increase in Western Cordilleran sources, all locations to the south show an increase in Eastern Cordilleran sources in the Cenozoic. Eastern Cordilleran sources become a significant (i.e., >50 ± 5%) proportion of the model at younger ages to the south. Data for this figure are available in Supplemental Table 10.

belt in the Western Cordillera provides a progressively greater proportion of detritus. In contrast, there is an upsection increase in Eastern Cordilleran-derived zircons in Cenozoic strata at all locations south of Cusco (Fig. 5). The second undocumented trend is that the model attributes a significant proportion of the age distribution to Eastern Cordilleran-derived sources at progressively younger ages to the south. This is highlighted by considering the age at which the model attributes >50 ± 5% of the zircon age distribution to Eastern Cordilleran sources. This occurs between 63.5 Ma and 57.3 Ma at 15°S (Llalli), between 54.7 Ma and 45.9 Ma at 16°S (Puno), between 65 and 44.2 Ma at 16.4°S (Juli), between 64.5 and 38.3 Ma at 16.5°S (Desaguadero), between 38.1 and 24.3 Ma at 16.6°S (Tiahuanacu), and between ~40 Ma and 36.7 Ma at 18°S (Chuquichambi) (Fig. 5).

5.3. Synthesis and tectonic model

The record of basin reorganization documented above can be compared to records of deformation and magmatism to assess geodynamic models. The termination of the unconformity and resumption of rapid sediment accumulation post-dates the thermochronologically determined timing of onset of exhumation of the Eastern Cordillera at the same latitudes (Fig. 6). This pattern is the opposite of that predicted by a retroarc foreland basin model and indicates that, despite exhibiting archetypal convex-up sediment accumulation curves (Fig. 3a), the Altiplano region was not a simple retroarc foreland basin in the Eocene–Oligocene because there was deformation and exhumation to the east of the study areas prior to the resumption of rapid sediment accumulation. Our data do not differentiate between models invoking an integrated Eastern Cordillera in which deformation is transferred from the Western Cordillera by a mid-crustal detachment (e.g., McQuarrie et al., 2008) verses two independent Western and Eastern cordilleran orogenic wedges (e.g., Martinod et al., 2020). However, neither model accounts for the 10–20 Myr nadir in sediment accumulation rate observed in the sediment accumulation records or its southward younging. Furthermore, comparing the timings of resumption of rapid sediment accumulation, Eastern Cordilleran exhumation, and a magmatic flare-up following a lull indicates that all three young to the south in lockstep (Fig. 7). We define the magmatic flare up as the westward expansion of magmatism that followed shut-down or waning of the Western Cordilleran magmatic arc and eastward migration of magmatism. As in the North American Cordillera, magmatism did not fully terminate, particularly at the eastern terminus of the flat slab (Constenius et al., 2003; Copeland et al., 2017) (Fig. 6 and Supplemental Data Table 11). All of this suggests that the observed Eocene–Oligocene condensed section is not a forebulge unconformity (Horton, 2022).

However, all of the observations outlined above are consistent with southward shallowing followed by resteepening of a flat or shallowly subducting slab (Fig. 8) (Runyon et al., 2021). Three primary factors control slab flattening (van Hunen et al., 2004; Liu and Currie, 2016): the absolute velocity of the overriding plate, the buoyancy of the subducting plate, and the magnitude of the dynamic suction force created by convection in the mantle wedge above the subducting plate. There was a decrease in absolute or westward motion of the South American plate between 60–40 Ma (Fig. 8f, Maloney et al., 2013), suggesting that the absolute velocity of the overriding plate was not a significant factor in slab flattening in this case. Furthermore, a change in plate velocity fails to explain the southward trend in deformation, magmatism, and sediment accumulation rates described above. Multiple studies have shown that the intersection between the Juan Fernandez Ridge and the Nazca Trench swept southward since ~40 Ma (Bello-González et al., 2018; Hu et al., 2021). However, prior to 40 Ma, the intersection migrated northward along the South American margin

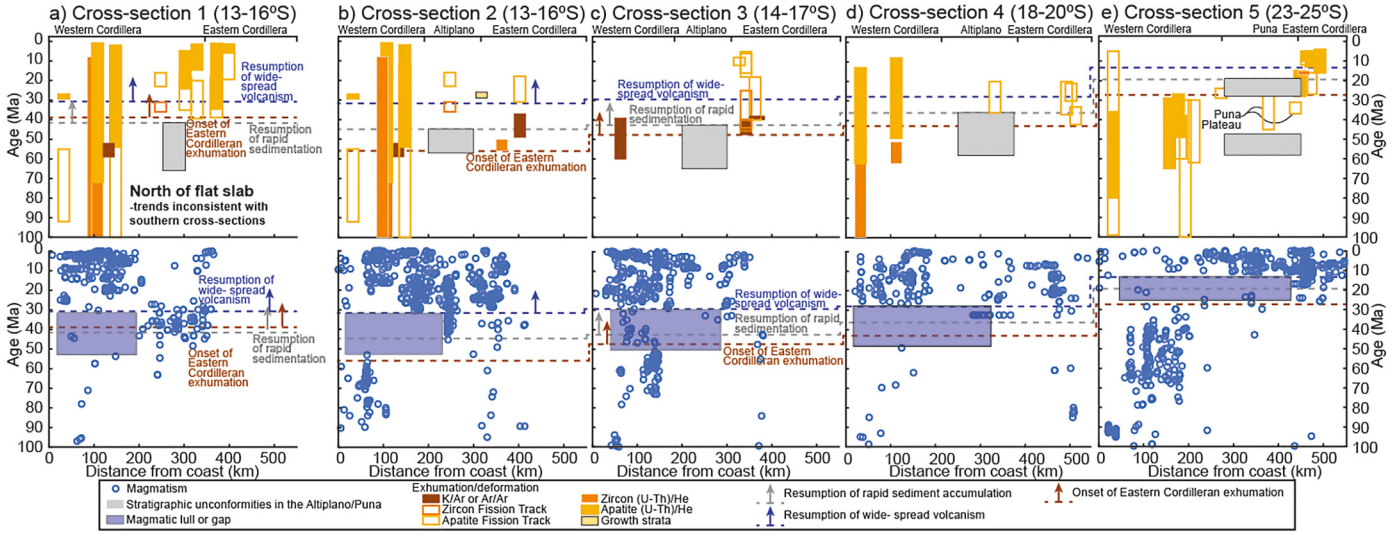

Fig. 6. Cross-sections showing the southward younging of magmatic lulls and flare-ups, exhumation, and unconformity development. The upper panels show exhumation and unconformity development, whereas the lower panels show magmatism. Trends are 100% opaque on their respective panels. Magmatism is projected onto cross sections along 100 km-wide swaths. Due to their proximity, the exhumation record for cross sections 1 and 2 is the same. Magmatism in cross-section 3 from 50–30 Ma is localized at the Bolivia-Chile border (see Fig. 8b and c). The location of cross-sections is shown in Fig. 8. Basin data are from this study. Thermochronology data are from McBride et al. (1987), Benjamin et al. (1987), Farrar et al. (1988), Clark et al. (1990), Kontak et al. (1990), Andriessen and Reutter (1994), Maksaev and Zentilli (1999), Carrapa et al. (2005, 2011, 2012, 2014), Deeken et al. (2006), Gillis et al. (2006), Scheuber et al. (2006), Ege et al. (2007), Barnes et al. (2008, 2012), McQuarrie et al. (2008), Wipf et al. (2008), Ruiz et al. (2009), Schildgen et al. (2009a), Gunnell et al. (2010), Juez-Larré et al. (2010), Eichelberger et al. (2013), Pearson et al. (2012), Perez and Horton (2014), Reiners et al. (2015), Anderson et al. (2018), Avdievitch et al. (2018), Henriquez et al. (2019; 2020), Perez and Levine (2020), Gérard et al. (2021a, 2021b) and Payrola et al. (2021). Magmatic data are from published data compiled by Pilger (2021). Compiled data are available in Supplemental Table 11.

due to its southward trending arm associated with migration of the Phoenix and Chazca plates over the Juan Fernandez Hotspot (Fig. 8). Nevertheless, there is no evidence for a northward migrating flat slab in the Paleocene–early Eocene. This suggests that the Juan Fernandez Ridge alone was insufficiently buoyant to drive slab flattening. Alternatively, plate models of the Manihiki Plateau suggest that if it was formed at the Tongareva Triple junction (Larson et al., 2002) it may have had a conjugate which would have collided with South America at the latitude of southern Peru at ~ 55 ± 5 Ma (O'Driscoll et al., 2012) (Fig. 8). This coincides in timing and location with the initial observations of slab flattening, suggesting that this larger feature may have been sufficiently buoyant

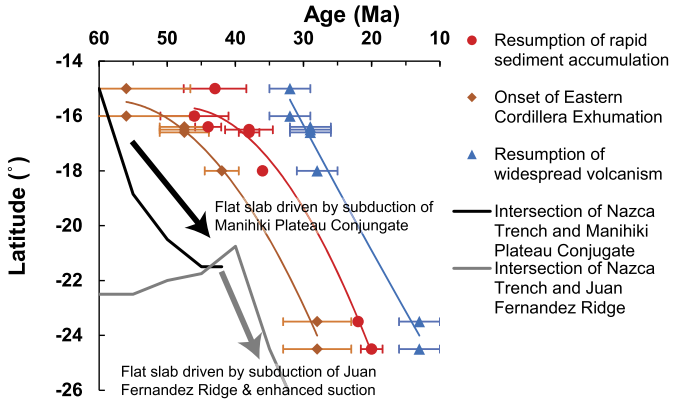

Fig. 7. Time-space relationship among onset of exhumation of the Eastern Cordillera, resumption of rapid sediment accumulation in the Altiplano-Puna Basin, the onset of a magmatic flare-up, and the trajectory of the intersection between the Nazca Trench and southern margin of the Manihiki Plateau Conjugate and Juan Fernandez Ridge. The timing for basin records is from Fig. 3 and error bars are based on uncertainties in calculated maximum depositional ages. The timing of exhumation in the Eastern Cordillera and timing of magmatic flare-up are from cross sections 2–5 in Fig. 6 and error bars are the larger of individual thermochronometric ages or the difference between individual thermochronometric ages and model ages. Error bars for the onset of magmatism were conservatively set at 3 Myr based on Fig. 6. Data for this figure are available in Supplemental Table 11.

to drive slab flattening. As the slab angle decreased, the suction force due to mantle convection in the narrowing space would have increased. As a result, when the Manihiki Plateau Conjugate was fully subducted and the Juan Fernandez Ridge began its southward sweep at ~40 Ma, flat subduction could have been maintained by the combined effects of ridge buoyancy and dynamic mantle suction (van Hunen et al., 2004) and would have migrated southward at the same pace as the Juan Fernandez Ridge (Fig. 8).

We therefore propose that the southward sweep in flat/shallow subduction was initiated by impingement of an anomalously thick oceanic plateau, such as a hypothetical Manihiki Plateau Conjugate, on the Nazca Trench (O'Driscoll et al., 2012). Plate reconstructions show that the proposed Manihiki Plateau Conjugate would have collided with South America in the Paleocene at the latitude of southern Peru (Fig. 8)(O'Driscoll et al., 2012) and subsequently the ridge/trench intersection would have migrated southward (Martinod et al., 2010; Bello-González et al., 2018; Hu et al., 2021). Hu et al. (2021) propose a similar southward migration of contractional deformation in response to southward migrating impingement of the buoyant Juan Fernandez Ridge on the Nazca Trench. The resumption of rapid sediment accumulation, initiation of a magmatic flare-up, and the initiation of contractional deformation in the Eastern Cordillera also migrate southward in lockstep with the Juan Fernandez Ridge intersection (Fig. 7). Increased coupling between the Nazca and South American plates due to sediment starvation in the trench alone is insufficient to account for the variety of upper plate effects documented in this study (Lamb and Davis, 2003). Specifically, the resumption of rapid sediment accumulation and magmatic flare-up, which occur 15–30 Myr after the impingement of the Juan Fernandez Ridge are difficult to attribute directly to the impact of enhanced interplate coupling. Southward slab flattening and resteepening in response to the southward sweep of the buoyant Juan Fernandez Ridge, however, provides a model that unifies all of the observations described above (Martinod et al., 2010).

Slab flattening caused an inboard jump in deformation from the Western Cordillera, seen in the timing of the onset of exhumation in the Eastern Cordillera (Fig. 6). The eastward jump

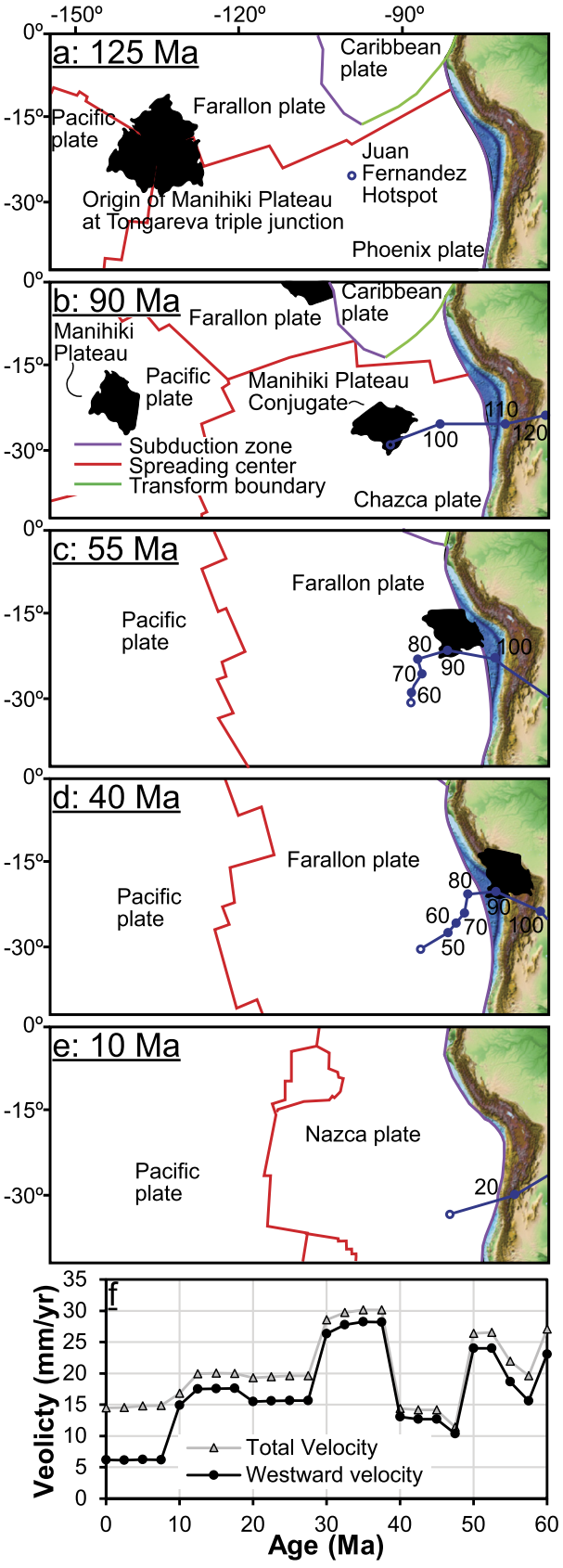

Fig. 8. a-e) Proposed tectonic evolution of the Manihiki Plateau based on the plateau origin model of Larson et al. (2002) and plate reconstructions by Müller et al. (2019). f) Velocity of a point at 17°S, 61°W, in the modern South American foreland in a fixed mantle reference frame using the plate reconstruction of Müller et al. (2019). Plate reconstruction implemented using GPlates 2.3 with a fixed South America reference frame (Müller et al., 2018).

in deformation resulted in a transition in the tectonic setting of the Altiplano/Puna region from a retroarc foreland basin to a hinterland basin (e.g., DeCelles et al., 2011; Carrapa and DeCelles, 2014). The model proposed herein predicts a variable lifespan of the retroarc foreland basin with a longer-lived foreland basin in the southern CAP than in the northern CAP due to southward slab flattening and migration of deformation into the Eastern Cordillera (Fig. 9), consistent with preservation of a forebulge unconformity at 23–26° (e.g., DeCelles et al., 2011). As seen with a southward migrating pulse of exhumation in the Western Cordillera in central Peru which accompanied the southward sweep in the Nazca Ridge (George et al., 2022), the model proposed here also predicts a southward migrating pulse of exhumation in the Western Cordillera that would accompany southward slab flattening. At the same time, slab flattening caused a shut-down or lull in the magmatic arc and a transient period of dynamic and/or isostatic uplift over the slab (Eakin et al., 2014b; Dávila and Lithgow-Bertelloni, 2015), resulting in formation of the observed Eocene unconformity or condensed section. Slab resteepening, potentially due to increased density following development of restite and/or eclogite, or because of crustal thickening in the overriding plate, occurred at progressively younger ages to the south and was accompanied by resumption of rapid sediment accumulation in the now hinterland Altiplano and Puna regions (Fig. 6). This southward migrating shallow subduction model suggests that emplacement of a flat slab beneath the CAP set the stage for plateau formation by focusing deformation on its eastern margin: it hydrated and weakened the Eastern Cordilleran crust and mantle lithosphere for later ductile lower crust deformation (Eichelberger et al., 2015; Garzione et al., 2017). The time between initial Eastern Cordilleran deformation and resteepening of the slab indicated by the magmatic flare-up predicts that the initial 10–20 Myr of Eastern Cordilleran shortening is directly linked to slab processes. Subsequent shortening may have been facilitated by continued deformation along lithospheric weaknesses developed in the Eastern Cordillera in those 10–20 Myr. The flat slab also thickened, hydrated, and weakened the CAP lithosphere (Humphreys, 2009), preparing it for subsequent delamination or convective removal inferred from younger sedimentary basin fill and in paleoaltimetry datasets (DeCelles et al., 2015b; Garzione et al., 2017; Sundell et al., 2019).

Progressive southward shallowing and resteepening of the slab accounts for several otherwise anomalous observations: the extreme CAP width, systematic magmatic waning followed by widespread magmatism, high-magnitude retroarc shortening, and anomalous basin subsidence. First, although the width of the CAP (Fig. 1) has been attributed to the presence of a thick Paleozoic stratigraphic package in the region of the Eastern Cordillera between ~15°S and 23°S (Allmendinger and Gubbels, 1996; McQuarrie, 2002), the zone of anomalous orogenic width extends both north and south of this zone (McGroder et al., 2015; Horton et al., 2022). In the model proposed above, the locus of initial Eastern Cordilleran deformation and hence the width of the CAP is explained by an increase in deviatoric stress in the crust overlying the hinge of a flat slab (Martinod et al., 2020), which may have reactivated lithospheric anisotropies such as the Permo-Triassic Mitu rift (Perez et al., 2016) or margins of the Arequipa Terrane (Dorbath et al., 1993; Mamani et al., 2008; Ramos, 2018). Progressive southward flattening of the slab provides a holistic context for observed southward decrease in cooling ages in the Eastern Cordillera (Fig. 6) and unifies previously proposed disparate episodes of slab flattening and steepening (Kay and Coira, 2009; Ramos, 2018). Second, slab flattening accounts for inboard migration of the magmatic arc at 50–45 Ma in southern Peru, the subsequent development of a magmatic gap at 15–19°S between 50 and 36 Ma (Fig. 3 and 4b), followed by diffuse volcanism in the Western Cordillera-Altiplano between 16°S and 26°S from 36–31 Ma (Sandeman et

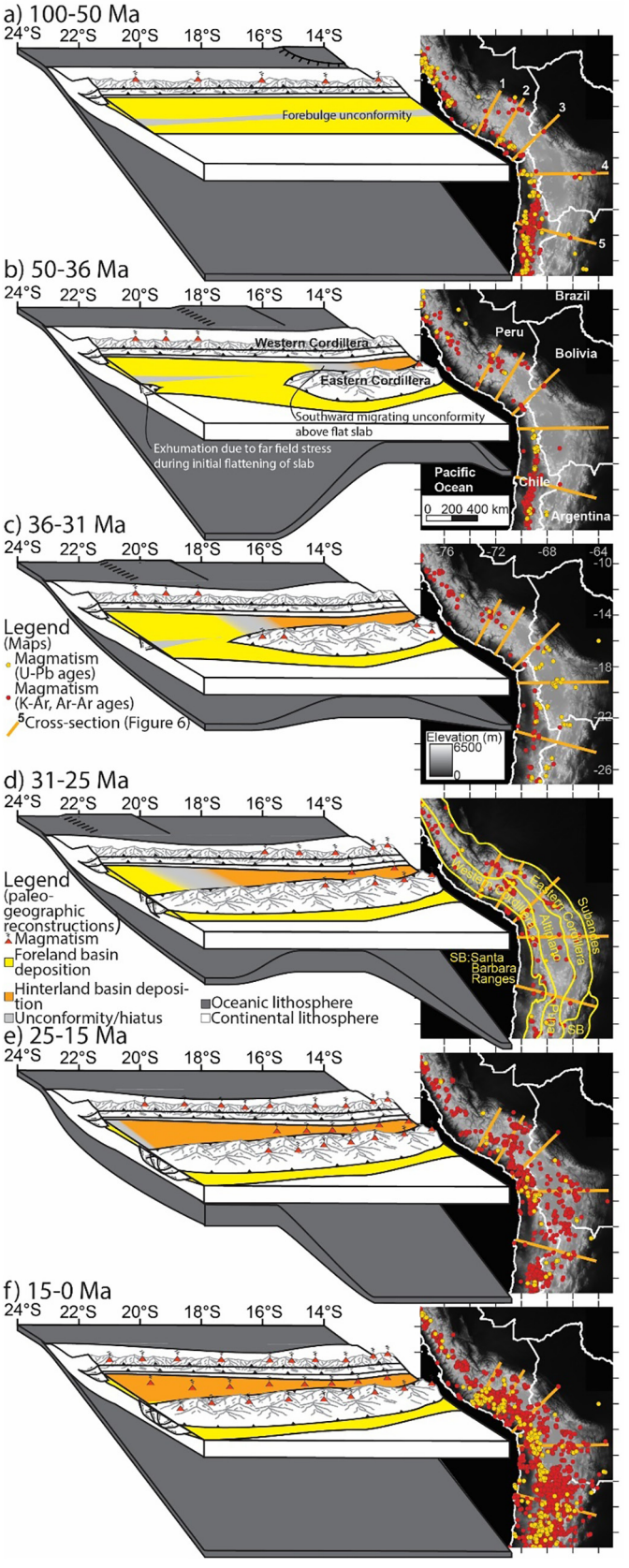

Fig. 9. Migration of the magmatic arc and 3D models of the evolution of the Altiplano-Puna flat slab through time.

al., 1995; Mamani et al., 2010; O'Driscoll et al., 2012) (Fig. 4c). This diffuse volcanism between 16°S and 26°S from 36–31 Ma suggests the presence of an asthenospheric wedge, implying that the slab may not have been fully flat at these latitudes and that a thin, wide, asthenospheric wedge persisted beneath at least parts of the Altiplano. Slab flattening is also associated with hydration and weakening of the overriding mantle lithosphere. In addition to facilitating shortening while the flat slab is in place, this hydration serves to initiate the widespread magmatism observed following passage of the unconformity (Fig. 6) and facilitate a transition of the lower crust to eclogite (Austrheim, 1998). Following removing of the flat slab, widespread melting of hydrated mantle or lower crust generated additional dense restite (e.g., Kay and Coira, 2009 and references therein). These two events conditioned the CAP lithosphere for later development of one or more Rayleigh-Taylor instabilities (Beck et al., 2014; Ward et al., 2016), which removed dense lithospheric material and resulted in isostatic surface uplift, creating the extreme topographic elevations that currently characterize the region (Garzione et al., 2017; Sundell et al., 2019; Göğüş et al., 2022). Third, slab flattening may have led to higher shortening in the upper plate via stronger coupling between the plates (Martinod et al., 2010; Horton, 2018b). Shortening was further enhanced by stratigraphic weaknesses introduced by the thick Bolivian Paleozoic stratigraphic wedge (Allmendinger and Gubbels, 1996; McQuarrie, 2002) and a hydration-weakened CAP lithosphere which accommodated westward transfer of crustal material during Eastern Cordilleran shortening (Eichelberger et al., 2015). The combination of flat subduction and inherited stratigraphic weakness can account for shortening magnitudes between ~16°S–24°S that exceed regions to the north or south (Gotberg et al., 2010; Eichelberger and McQuarrie, 2015). Fourth, this region exhibits magnitudes of sediment accumulation both greater than and less than predicted from surface geology (Perez and Levine, 2020; Runyon et al., 2021). The lateral transitions between flat and shallow subduction segments (Fig. 7), would introduce north-south variability in dynamic topography along the CAP (Gurnis, 1992). This may explain stratigraphic thicknesses that exceed or are less than accommodation predicted by flexure due to upper crustal (topographic) loading alone (Perez and Levine, 2020; Runyon et al., 2021).

5.4. Broader implications

The synthesis presented here demonstrates a southward-younging unconformity spanning ~14°–26°S that we attribute to reduced sediment accumulation during passage of a flat/shallow slab. Development of stratigraphic unconformities associated with flat subduction has been documented in other cordilleran settings, suggesting that it may constitute one element of a generalized model. For example, flat subduction also likely resulted in formation of Campanian unconformities (the Moxa Unconformities, Rudolph et al., 2015) in the proximal retroarc foreland basin in the North American Cordillera (Saylor et al., 2020; Davis et al., 2022) via isostatic or dynamic uplift above the flat portion of the slab.

Impingement of a buoyant oceanic plateau at ~14°S followed by progressive southward slab flattening and resteepening also resolves conflicting histories of deformation and basin formation at ~23–26°S. The conflict arises between models which invoke an irregular progression of deformation (e.g., Strecker et al., 2011) and those which envision the development of the Puna plateau as the result of a progressive eastward propagating fold-thrust belt or deformation front and associated retroarc foreland basin (DeCelles et al., 2011; Carrapa et al., 2012). We suggest a synthesis in which the minor Eocene deformation in the Eastern Cordillera of the southern CAP indicated by partially reset Eocene zircon (U-Th)/He ages (Pearson et al., 2012) and minor Eocene exhumation identified in apatite fission track age models (Deeken et al., 2006) may be caused by far-field contractional stresses in the upper plate associated with slab flattening (Livaccari and Perry, 1993; Axen et al.,

2018). However, following slab flattening and prior to arrival of the flat slab in the eastern Puna Plateau, deformation waned and the region was reincorporated into a regional retroarc foreland basin. This model of far-field deformation is similar to that proposed by Saylor et al. (2020) to account for Cenomanian–Turonian exhumation of basement-cored uplifts in the retroarc Laramide province of the North American cordillera (Carrapa et al., 2019) prior to its reincorporation into the regional foreland basin system. Localization of strain prior to arrival of the flat slab suggests that far-field contractional stresses deformed pre-existing lithospheric anisotropies in the Argentinian Eastern Cordillera and Montana Laramide province as predicted by geodynamic models (e.g., Axen et al., 2018). These similarities suggest that reactivation of lithospheric anisotropies in response to far field stresses is a common element during the initial stages of flat slab or shallow subduction.

6. Conclusion

The new detrital zircon maximum depositional ages presented herein document a southward migrating Eocene–early Miocene unconformity in Altiplano and Puna basins separating Paleogene–Cretaceous retroarc foreland basin strata or pre-Upper Cretaceous pre-orogenic strata below from hinterland basin strata above. This unconformity occurs in early Eocene strata at ~14-16°S but in strata as young as Oligocene–early Miocene at ~23–26°S. Inverse and forward modelling of detrital zircon provenance data suggests Paleogene introduction of Eastern Cordilleran detritus between 15°S–18°S. Modelling also indicates that the Eastern Cordillera became a significant contributor to Altiplano Basin strata at progressively younger ages to the south.

The southward migrating unconformity and introduction of Eastern Cordilleran detritus occurs in lockstep with southward migration of magmatic lulls, widening of the magmatic arc, and migration of deformation into the Eastern Cordillera. We propose that all of these features can be explained within a unified model invoking a southward migrating Paleogene-early Neogene flat/shallow slab. The timing, locus and pace of southward migration of exhumation, resumption of rapid sediment accumulation, and magmatic flare up is consistent with plate models of the impingement of a Manihiki Plateau Conjugate on the Nazca Trench, suggesting that it is responsible for initial slab flattening. Subsequent upper plate effects track the southward migration of the Juan Fernandez Ridge, suggesting that this buoyant asperity coupled with enhanced dynamic mantle suction may have been responsible for maintaining flat slab subduction and its southward migration. The emplacement and removal of a flat slab identified by this multidisciplinary approach corresponds to the region of anomalously thick crust, high elevations, and extreme orogenic width that characterizes the Central Andean Plateau.

We suggest that the central Andean crust was hydrated and weakened by the emplacement and removal of flat/shallow subduction that facilitated subsequent high-magnitude crustal shortening, attendant crustal thickening, and defined the plateau width. Conditioning of the Andean crust via flat subduction provides a unified hypothesis for the development of the world's largest non-collisional plateau. As an analog for ancient plateaux in other cordilleran settings around the world, this conclusion suggests that plateau development in cordilleran settings is controlled by the impact of lower plate processes (slab angle), on upper plate processes such as inherited crustal anisotropies and inherited stratigraphic architecture.

CRediT authorship contribution statement

Joel Saylor: Conceptualization, Funding acquisition, Field work, Writing, Supervision
Kurt Sundell: Conceptualization, Investigation, Writing
Nicholas Perez: Conceptualization, Field work, Writing
Jeffrey Hensley: Field work, Investigation, Visualization
Payton McCain: Field work, Investigation, Visualization
Brook Runyon: Field work, Investigation, Visualization
Paola Alvarez: Field work, Consultation
José Cárdenas: Resources, Consultation
Whitney Usnayo: Field work, Consultation
Carlos Valer: Field work

Declaration of competing interest

The authors declare that they have no known competing financial interests or personal relationships that could have appeared to influence the work reported in this paper.

Data availability

All data are available in the Supplemental Tables and in publicly accessible online databases.

Acknowledgements

This research was supported by a grant from the National Science Foundation (EAR-1550097), funding from the University of British Columbia, and a Discovery grant from the Natural Science and Engineering Research Council (RGPIN-2020-04691). We are grateful to Editor A. Webb for handling this manuscript and an anonymous reviewer and N. McQuarrie for detailed reviews. We also thank A. Stevens Goddard for comments on an earlier version of this manuscript.

Appendix A. Supplementary material

Supplementary material related to this article can be found online at https://doi.org/10.1016/j.epsl.2023.118050.

References

Allmendinger, R., Gubbels, T., 1996. Pure and simple shear plateau uplift, Altiplano-Puna, Argentina and Bolivia. Tectonophysics 259, 1–13.
Anderson, R., Long, S., Horton, B., Thomson, S., Calle, A., Stockli, D., 2018. Orogenic wedge evolution of the central Andes, Bolivia (21°S): implications for Cordilleran cyclicity. Tectonics 37, 3577–3609.
Andriessen, P.A., Reutter, K.-J., 1994. K-Ar and fission track mineral age determination of igneous rocks related to multiple magmatic arc systems along the 23°S latitude of Chile and NW Argentina. In: Tectonics of the Southern Central Andes. Springer, pp. 141–153.
Arriagada, C., Roperch, P., Mpodozis, C., Fernandez, R., 2006. Paleomagnetism and tectonics of the southern Atacama Desert (25–28 °S), northern Chile. Tectonics 25.
Arriagada, C., Roperch, P., Mpodozis, C., Cobbold, P.R., 2008. Paleogene building of the Bolivian Orocline: tectonic restoration of the central Andes in 2-D map view. Tectonics 27.
Austrheim, H., 1998. Influence of fluid and deformation on metamorphism of the deep crust and consequences for the geodynamics of collision zones. In: Hacker, B.R., Liou, J.G. (Eds.), When Continents Collide: Geodynamics and Geochemistry of Ultrahigh-Pressure Rocks. Springer, Netherlands, Dordrecht, pp. 297–323.
Avdievitch, N.N., Ehlers, T.A., Glotzbach, C., 2018. Slow long-term exhumation of the West central Andean plate boundary, Chile. Tectonics 37, 2243–2267.
Axen, G.J., van Wijk, J.W., Currie, C.A., 2018. Basal continental mantle lithosphere displaced by flat-slab subduction. Nat. Geosci. 11, 961–964.
Bahlburg, H., Vervoort, J.D., Du Frane, S.A., Bock, B., Augustsson, C., Reimann, C., 2009. Timing of crust formation and recycling in accretionary orogens: insights learned from the western margin of South America. Earth-Sci. Rev. 97, 215–241.
Barnes, J.B., Ehlers, T.A., McQuarrie, N., O'Sullivan, P.B., Tawackoli, S., 2008. Thermochronometer record of central Andean plateau growth, Bolivia (19.5 degrees S). Tectonics 27.
Barnes, J.B., Ehlers, T.A., 2009. End member models for Andean Plateau uplift. Earth-Sci. Rev. 97, 105–132.
Barnes, J.B., Ehlers, T.A., Insel, N., McQuarrie, N., Poulsen, C.J., 2012. Linking orography, climate, and exhumation across the central Andes. Geology 40, 1135–1138.

Beck, S.L., Zandt, G., Ward, K.M., Scire, A., 2014. Multiple Styles and Scales of Lithospheric Foundering Beneath the Puna Plateau, Central Andes. Geological Society of America Memoirs, vol. 212.
Bello-González, J.P., Contreras-Reyes, E., Arriagada, C., 2018. Predicted path for hotspot tracks off South America since Paleocene times: tectonic implications of ridge-trench collision along the Andean margin. Gondwana Res. 64, 216–234.
Benjamin, M.T., Johnson, N.M., Naeser, C.W., 1987. Recent rapid uplift in the Bolivian Andes: evidence from fission-track dating. Geology 15, 680–683.
Bird, P., 1998. Kinematic history of the Laramide orogeny in latitudes 35°–49°N, western United States. Tectonics 17, 780–801.
Brown, W.G., Schmidt, C., Perry, W., 1988. Deformational Style of Laramide Uplifts in the Wyoming Foreland. Interaction of the Rocky Mountain Foreland and the Cordilleran Thrust Belt, vol. 171. Geological Society of America Memoir, pp. 1–25.
Buford-Parks, V.M., McQuarrie, N., 2019. Kinematic, flexural, and thermal modelling in the Central Andes: unravelling age and signal of deformation, exhumation, and uplift. Tectonophysics 766, 302–325.
Carlotto, V., Jaillard, E., Mascle, G., 1992. Relación entre sedimentación, paleogeografía y tectónica en la región de Cusco (sur del Perú) entre el Jurásico superior - Paleoceno. In: Boletín Sociedad Geológica del Perú, vol. 83, pp. 1–20.
Carlotto, V., Carlier, G., Jaillard, E., Mascle, G., Cárdenas, J., Fornari, M., Cerpa, L., 2002. Paleogeographic control in the evolution of Tertiary Basins in the Western Cordillera and Altiplano of southern Peru (Condoroma-Cusco-Ayaviri). In: 5th Intern, Symp. and Geodyn. ISAG, Tolouse, France. ORSTOM ed.
Carlotto, V., 2013. Paleogeographic and tectonic controls on the evolution of Cenozoic basins in the Altiplano and Western Cordillera of southern Peru. Tectonophysics 589, 195–219.
Carrapa, B., Adelmann, D., Hilley, G., Mortimer, E., Sobel, E., Strecker, M., 2005. Oligocene range uplift and development of plateau morphology in the southern central Andes. Tectonics 24.
Carrapa, B., Trimble, J.D., Stockli, D.F., 2011. Patterns and timing of exhumation and deformation in the Eastern Cordillera of NW Argentina revealed by (U-Th)/He thermochronology. Tectonics 30.
Carrapa, B., Bywater-Reyes, S., DeCelles, P.G., Mortimer, E., Gehrels, G.E., 2012. Late Eocene–Pliocene basin evolution in the Eastern Cordillera of northwestern Argentina (25°–26°S): regional implications for Andean orogenic wedge development. Basin Res. 24, 249–268.
Carrapa, B., DeCelles, P.G., 2014. Regional exhumation and kinematic history of the central Andes in response to cyclical orogenic processes. In: Geological Society of America Memoirs, vol. 212.
Carrapa, B., Reyes-Bywater, S., Safipour, R., Sobel, E.R., Schoenbohm, L.M., DeCelles, P.G., Reiners, P.W., Stockli, D., 2014. The effect of inherited paleotopography on exhumation of the Central Andes of NW Argentina. Geol. Soc. Am. Bull. 126, 66–77.
Carrapa, B., DeCelles, P.G., Romero, M., 2019. Early inception of the Laramide Orogeny in southwestern Montana and northern Wyoming: implications for models of flat-slab subduction. J. Geophys. Res., Solid Earth 124, 2102–2123.
Clark, A.H., Farrar, E., Kontak, D.J., Langridge, R.J., Arenas F., M.J., France, L.J., McBride, S.L., Woodman, P.L., Wasteneys, H.A., Sandeman, H.A., Archibald, D.A., 1990. Geologic and geochronologic constraints on the metallogenic evolution of the Andes of southeastern Peru. Econ. Geol. 85, 1520–1583.
Coney, P.J., Reynolds, S.J., 1977. Cordilleran Benioff zones. Nature 270, 403.
Constenius, K.N., Esser, R.P., Layer, P.W., 2003. Extensional collapse of the Charleston-Nebo Salient and its relationship to space-time variations in Cordilleran orogenic belt tectonism and continental stratigraphy. In: Raynolds, R.G., Flores, R.M. (Eds.), Cenozoic Systems of the Rocky Mountain Region. Rocky Mountain SEPM, Denver, pp. 303–353.
Copeland, P., Currie, C.A., Lawton, T.F., Murphy, M.A., 2017. Location, location, location: the variable lifespan of the Laramide orogeny. Geology 45, 223–226.
Coutts, D.S., Matthews, W.A., Hubbard, S.M., 2019. Assessment of widely used methods to derive depositional ages from detrital zircon populations. Geosci. Front. 10, 1421–1435.
Dávila, F.M., Lithgow-Bertelloni, C., 2015. Dynamic uplift during slab flattening. Earth Planet. Sci. Lett. 425, 34–43.
Davis, E.M., Rudolph, K.W., Saylor, J.E., Lapen, T.J., Wellner, J.S., 2022. Effects of contemporaneous orogenesis on sedimentation in the Late Cretaceous Western Interior Basin, northern Utah and southwestern Wyoming. Basin Res. 34, 366–392.
DeCelles, P., Carrapa, B., Gehrels, G., 2007. Detrital zircon U-Pb ages provide provenance and chronostratigraphic information from Eocene synorogenic deposits in northwestern Argentina. Geology 35, 323–326.
DeCelles, P.G., Horton, B.K., 2003. Early to middle Tertiary foreland basin development and the history of Andean crustal shortening in Bolivia. Geol. Soc. Am. Bull. 115, 58–77.
DeCelles, P.G., Ducea, M.N., Kapp, P., Zandt, G., 2009. Cyclicity in Cordilleran orogenic systems. Nat. Geosci. 2, 251–257.
DeCelles, P.G., Carrapa, B., Horton, B.K., Gehrels, G.E., 2011. Cenozoic foreland basin system in the central Andes of northwestern Argentina: implications for Andean geodynamics and modes of deformation. Tectonics 30.
DeCelles, P.G., Carrapa, B., Horton, B., McNabb, J., Gehrels, G.E., Boyd, J., 2015a. The Miocene Arizaro Basin, Central Andean Hinterland: Response to Partial Lithosphere Removal. Geodynamics of a Cordilleran Orogenic System: The Central Andes of Argentina and Northern Chile, vol. 212. Geological Society of America Memoir, pp. 359–386.
DeCelles, P.G., Carrapa, B., Horton, B.K., McNabb, J., Gehrels, G.E., Boyd, J., 2015b. The Miocene Arizaro Basin, central Andean hinterland: response to partial lithosphere removal? In: Geological Society of America Memoirs, vol. 212.
Deeken, A., Sobel, E.R., Coutand, I., Haschke, M., Riller, U., Strecker, M.R., 2006. Development of the southern Eastern Cordillera, NW Argentina, constrained by apatite fission track thermochronology: from early Cretaceous extension to middle Miocene shortening. Tectonics 25.
del Papa, C.E., Salfity, J., 1999. Non-marine Paleogene sequences, Salta group, Northwest Argentina. Acta Geol. Hisp., 105–121.
Dorbath, C., Granet, M., Poupinet, G., Martinez, C., 1993. A teleseismic study of the Altiplano and the Eastern Cordillera in northern Bolivia: new constraints on a lithospheric model. J. Geophys. Res., Solid Earth 98, 9825–9844.
Eakin, C.M., Lithgow-Bertelloni, C., Dávila, F.M., 2014a. Influence of Peruvian flat-subduction dynamics on the evolution of western Amazonia. Earth Planet. Sci. Lett. 404, 250–260.
Eakin, C.M., Long, M.D., Beck, S.L., Wagner, L.S., Tavera, H., Condori, C., 2014b. Response of the mantle to flat slab evolution: insights from local S splitting beneath Peru. Geophys. Res. Lett. 41, 3438–3446.
Ege, H., Sobel, E.R., Scheuber, E., Jacobshagen, V., 2007. Exhumation history of the southern Altiplano plateau (southern Bolivia) constrained by apatite fission track thermochronology. Tectonics 26, TC1004.
Eichelberger, N., McQuarrie, N., Ehlers, T.A., Enkelmann, E., Barnes, J.B., Lease, R.O., 2013. New constraints on the chronology, magnitude, and distribution of deformation within the central Andean orocline. Tectonics 32, 1432–1453.
Eichelberger, N., McQuarrie, N., 2015. Kinematic reconstruction of the Bolivian orocline. Geosphere 11, 445–462.
Eichelberger, N., McQuarrie, N., Ryan, J., Karimi, B., Beck, S., Zandt, G., 2015. Evolution of crustal thickening in the central Andes, Bolivia. Earth Planet. Sci. Lett. 426, 191–203.
Farrar, E., Clark, A.H., Kontak, D.J., Archibald, D.A., 1988. Zongo-San Gabán zone: Eocene foreland boundary of the Central Andean orogen, northwest Bolivia and southeast Peru. Geology 16, 55–58.
Flament, N., Gurnis, M., Müller, R.D., Bower, D.J., Husson, L., 2015. Influence of subduction history on South American topography. Earth Planet. Sci. Lett. 430, 9–18.
Fornari, M., Baldellón, E., Espinoza, F., Ibarra, I., Jiménez, N., Mamani, M., 2002. Ar\Ar dating of late Oligocene–early Miocene volcanism in the Altiplano. In: 5th International Symposium on Andean Geodynamics. Toulouse, France, pp. 223–226.
Garzione, C.N., McQuarrie, N., Perez, N.D., Ehlers, T.A., Beck, S.L., Kar, N., Eichelberger, N., Chapman, A.D., Ward, K.M., Ducea, M.N., Lease, R.O., Poulsen, C.J., Wagner, L.S., Saylor, J.E., Zandt, G., Horton, B.K., 2017. Tectonic evolution of the Central Andean Plateau and implications for the growth of plateaus. Annu. Rev. Earth Planet. Sci. 45, 529–559.
Gayet, M., Marshall, L., Sempéré, T., 1991. The Mesozoic and Paleocene vertebrates of Bolivia and their stratigraphic context: a review. Rev. Téc. Yacim. Pet. Fisc. Boliv. 12, 393–433.
George, S.W.M., Perez, N.D., Struble, W., Curry, M.E., Horton, B.K., 2022. Aseismic ridge subduction focused late Cenozoic exhumation above the Peruvian flat slab. Earth Planet. Sci. Lett. 600, 117754.
Gérard, B., Audin, L., Robert, X., Gautheron, C., van der Beek, P., Bernet, M., Benavente, C., Delgado, F., 2021a. Pliocene river capture and incision of the northern Altiplano: Machu Picchu, Peru. J. Geol. Soc. 178.
Gérard, B., Robert, X., Audin, L., Valla, P.G., Bernet, M., Gautheron, C., 2021b. Differential exhumation of the Eastern Cordillera in the Central Andes: evidence for South-Verging Backthrusting (Abancay Deflection, Peru). Tectonics 40, e2020TC006314.
Gillis, R.J., Horton, B.K., Grove, M., 2006. Thermochronology, geochronology, and upper crustal structure of the Cordillera real: implications for Cenozoic exhumation of the central Andean plateau. Tectonics 25, TC6007.
Göğüş, O.H., Sundell, K., Uluocak, E.Ş., Saylor, J., Çetiner, U., 2022. Rapid surface uplift and crustal flow in the Central Andes (southern Peru) controlled by lithospheric drip dynamics. Sci. Rep. 12, 5500.
Gotberg, N., McQuarrie, N., Caillaux, V.C., 2010. Comparison of crustal thickening budget and shortening estimates in southern Peru (12-14 degrees S): implications for mass balance and rotations in the “Bolivian orocline”. Geol. Soc. Am. Bull. 122, 727–742.
Gunnell, Y., Thouret, J.-C., Brichau, S., Carter, A., Gallagher, K., 2010. Low-temperature thermochronology in the Peruvian Central Andes: implications for long-term continental denudation, timing of plateau uplift, canyon incision and lithosphere dynamics. J. Geol. Soc. 167, 803–815.
Gurnis, M., 1992. Rapid continental subsidence following the initiation and evolution of subduction. Science 255, 1556–1558.
Henriquez, S., DeCelles, P.G., Carrapa, B., 2019. Cretaceous to middle Cenozoic exhumation history of the Cordillera de Domeyko and Salar de Atacama basin, northern Chile. Tectonics 38, 395–416.
Henríquez, S., DeCelles, P.G., Carrapa, B., Hughes, A.N., Davis, G.H., Alvarado, P., 2020. Deformation history of the Puna plateau, Central Andes of northwestern Argentina. J. Struct. Geol. 140, 104133.

Hongn, F., d. Papa, C., Powell, J., Petrinovic, I., Mon, R., Deraco, V., 2007. Middle Eocene deformation and sedimentation in the Puna-Eastern Cordillera transition (23-26°S): control by preexisting heterogeneities on the pattern of initial Andean shortening. Geology 35, 271–274.
Horton, B.K., Hampton, B.A., Waanders, G.L., 2001. Paleogene synorogenic sedimentation in the Altiplano plateau and implications for initial mountain building in the central Andes. Geol. Soc. Am. Bull. 113, 1387–1400.
Horton, B.K., Perez, N.D., Fitch, J.D., Saylor, J.E., 2015. Punctuated shortening and subsidence in the Altiplano Plateau of southern Peru: implications for early Andean mountain building. Lithosphere 7, 117–137.
Horton, B.K., 2018a. Sedimentary record of Andean mountain building. Earth-Sci. Rev. 178, 279–309.
Horton, B.K., 2018b. Tectonic regimes of the central and southern Andes: responses to variations in plate coupling during subduction. Tectonics 37, 402–429.
Horton, B.K., 2022. Unconformity development in retroarc foreland basins: implications for the geodynamics of Andean-type margins. J. Geol. Soc. 179.
Horton, B.K., Capaldi, T.N., Perez, N.D., 2022. The role of flat slab subduction, ridge subduction, and tectonic inheritance in Andean deformation. Geology.
Hu, J., Liu, L., Gurnis, M., 2021. Southward expanding plate coupling due to variation in sediment subduction as a cause of Andean growth. Nat. Commun. 12, 1–9.
Humphreys, E., 2009. Relation of flat subduction to magmatism and deformation in the western United States. In: Kay, S.M., Ramos, V.A., Dickinson, W.R. (Eds.), Backbone of the Americas: Shallow Subduction, Plateau Uplift, and Ridge and Terrane Collision. Geological Society of America, Boulder, CO, pp. 85–98.
Jadamec, M.A., Billen, M.I., Roeske, S.M., 2013. Three-dimensional numerical models of flat slab subduction and the Denali fault driving deformation in south-central Alaska. Earth Planet. Sci. Lett. 376, 29–42.
Jaillard, E., Feist, M., Grambast-Fessard, N., Carlotto, V., 1994. Senonian-Paleocene charophyte succession of the Peruvian Andes. Cretac. Res. 15, 445–456.
James, D.E., Sacks, S., 1999. Cenozoic formation of the central Andes: a geophysical perspective. In: Skinner, B. (Ed.), Geology and Ore Deposits of the Central Andes. Society of Economic Geologists, Littleton, CO, pp. 1–25.
Jiménez, N., López-Velásquez, S., Santiváñez, R., 2009. Evolución tectonomagmática de los Andes Bolivianos. Rev. Asoc. Geol. Argent. 65, 036.
Juez-Larré, J., Kukowski, N., Dunai, T.J., Hartley, A.J., Andriessen, P.A., 2010. Thermal and exhumation history of the Coastal Cordillera arc of northern Chile revealed by thermochronological dating. Tectonophysics 495, 48–66.
Kay, S.M., Coira, B.L., 2009. Shallowing and steepening subduction zones, continental lithospheric loss, magmatism, and crustal fl ow under the Central Andean Altiplano-Puna Plateau. In: Kay, S.M., Ramos, V.A., Dickinson, W.R. (Eds.), Backbone of the Americas: Shallow Subduction, Plateau Uplift, and Ridge and Terrane Collision. Geological Society of America, Boulder, pp. 229–259.
Kontak, D.J., Farrar, E., Clark, A.H., Archibald, D.A., 1990. Eocene tectono-thermal rejuvenation of an upper Paleozoic-lower Mesozoic terrane in the Cordillera de Carabaya, Puno, southeastern Peru, revealed by K · Ar and 40Ar/39Ar dating. J. South Am. Earth Sci. 3, 231–246.
Lamb, S., Davis, P., 2003. Cenozoic climate change as a possible cause for the rise of the Andes. Nature 425, 792–797.
Larson, R.L., Pockalny, R.A., Viso, R.F., Erba, E., Abrams, L.J., Luyendyk, B.P., Stock, J.M., Clayton, R.W., 2002. Mid-Cretaceous tectonic evolution of the Tongareva triple junction in the southwestern Pacific Basin. Geology 30, 67–70.
Leier, A.L., McQuarrie, N., Horton, B.K., Gehrels, G.E., 2010. Upper Oligocene conglomerates of the Altiplano, central Andes: the record of deposition and deformation along the margin of a hinterland basin. J. Sediment. Res. 80, 750–762.
Liu, S., Nummedal, D., Liu, L., 2011. Migration of dynamic subsidence across the Late Cretaceous United States Western Interior Basin in response to Farallon plate subduction. Geology 39, 555–558.
Liu, S., Currie, C.A., 2016. Farallon plate dynamics prior to the Laramide orogeny: numerical models of flat subduction. Tectonophysics 666, 33–47.
Livaccari, R.F., Perry, F.V., 1993. Isotopic evidence for preservation of Cordilleran lithospheric mantle during the Sevier-Laramide orogeny, western United States. Geology 21, 719–722.
Maksaev, V., Zentilli, M., 1999. Fission track thermochronology of the Domeyko Cordillera, northern Chile: Implications for Andean tectonics and porphyry copper metallogenesis. Explor. Min. Geol. 8, 65–90.
Maloney, K.T., Clarke, G.L., Klepeis, K.A., Quevedo, L., 2013. The Late Jurassic to present evolution of the Andean margin: drivers and the geological record. Tectonics 32, 1049–1065.
Mamani, M., Tassara, A., Wörner, G., 2008. Composition and structural control of crustal domains in the central Andes. Geochem. Geophys. Geosyst. 9.
Mamani, M., Worner, G., Sempere, T., 2010. Geochemical variations in igneous rocks of the Central Andean orocline (13 degrees S to 18 degrees S): tracing crustal thickening and magma generation through time and space. Geol. Soc. Am. Bull. 122, 162–182.
Margirier, A., Robert, X., Audin, L., Gautheron, C., Bernet, M., Hall, S., Simon-Labric, T., 2015. Slab flattening, magmatism, and surface uplift in the Cordillera Occidental (northern Peru). Geology 43, 1031–1034.
Martinod, J., Husson, L., Roperch, P., Guillaume, B., Espurt, N., 2010. Horizontal subduction zones, convergence velocity and the building of the Andes. Earth Planet. Sci. Lett. 299, 299–309.
Martinod, J., Gérault, M., Husson, L., Regard, V., 2020. Widening of the Andes: an interplay between subduction dynamics and crustal wedge tectonics. Earth-Sci. Rev. 204, 103170.
McBride, S.L., Clark, A.H., Farrar, E., Archibald, D.A., 1987. Delimitation of a cryptic Eocene tectono-thermal domain in the Eastern Cordillera of the Bolivian Andes through K–Ar dating and 40Ar–39Ar step-heating. J. Geol. Soc. 144, 243–255.
McGroder, M.F., Lease, R.O., Pearson, D.M., 2015. Along-strike variation in structural styles and hydrocarbon occurrences, Subandean fold-and-thrust belt and inner foreland, Colombia to Argentina. In: DeCelles, P.G., Ducea, M.N., Carrapa, B., Kapp, P.A. (Eds.), Eodynamics of a Cordilleran Orogenic System: The Central Andes of Argentina and Northern Chile. The Geological Society of America, pp. 79–114.
McQuarrie, N., 2002. Initial plate geometry, shortening variations, and evolution of the Bolivian orocline. Geology 30, 867–870.
McQuarrie, N., Horton, B.K., Zandt, G., Beck, S., DeCelles, P.G., 2005. Lithospheric evolution of the Andean fold-thrust belt, Bolivia, and the origin of the central Andean plateau. Tectonophysics 399, 15–37.
McQuarrie, N., Barnes, J.B., Ehlers, T.A., 2008. Geometric, kinematic, and erosional history of the central Andean Plateau, Bolivia (15-17 degrees S). Tectonics 27.
Müller, R.D., Cannon, J., Qin, X., Watson, R.J., Gurnis, M., Williams, S., Pfaffelmoser, T., Seton, M., Russell, S.H., Zahirovic, S., 2018. GPlates: building a virtual Earth through deep time. Geochem. Geophys. Geosyst. 19, 2243–2261.
Müller, R.D., Zahirovic, S., Williams, S.E., Cannon, J., Seton, M., Bower, D.J., Tetley, M.G., Heine, C., Le Breton, E., Liu, S., 2019. A global plate model including lithospheric deformation along major rifts and orogens since the Triassic. Tectonics 38, 1884–1907.
O'Driscoll, L.J., Richards, M.A., Humphreys, E.D., 2012. Nazca-South America interactions and the late Eocene-late Oligocene flat-slab episode in the central Andes. Tectonics 31.
Payrola, P., Zapata, S., Sobel, E.R., d. Papa, C., Pingel, H., Glodny, J., Ledesma, J., 2021. Exhumation and structural evolution of the high-elevation Malcante Range, Eastern Cordillera, NW Argentina. J. South Am. Earth Sci. 105, 102990.
Pearson, D., Kapp, P., Reiners, P., Gehrels, G., Ducea, M., Pullen, A., Otamendi, J.E., Alonso, R.N., 2012. Major Miocene exhumation by fault-propagation folding within a metamorphosed, early Paleozoic thrust belt, Northwestern Argentina. Tectonics 31.
Perez, N.D., Horton, B.K., 2014. Oligocene-Miocene deformational and depositional history of the Andean hinterland basin in the northern Altiplano plateau, southern Peru. Tectonics 33, 2014TC003647.
Perez, N.D., Horton, B.K., Carlotto, V., 2016. Structural inheritance and selective reactivation in the central Andes: Cenozoic deformation guided by pre-Andean structures in southern Peru. Tectonophysics 671, 264–280.
Perez, N.D., Levine, K.G., 2020. Diagnosing an ancient shallow-angle subduction event from Cenozoic depositional and deformational records in the central Andes of southern Peru. Earth Planet. Sci. Lett. 541, 116263.
Pilger, R., 2021. Radiometric Ages from the South American Andes.
Rak, A.J., McQuarrie, N., Ehlers, T.A., 2017. Kinematics, exhumation, and sedimentation of the North Central Andes (Bolivia): an integrated thermochronometer and thermokinematic modeling approach. Tectonics 36, 2524–2554.
Ramos, V.A., 2018. Tectonic evolution of the Central Andes: from terrane accretion to crustal delamination. In: Zamora, G., McClay, K.M., Ramos, V.A. (Eds.), Petroleum Basins and Hydrocarbon Potential of the Andes of Peru and Bolivia. American Association of Petroleum Geologists, pp. 1–34.
Reimann, C.R., Bahlburg, H., Kooijman, E., Berndt, J., Gerdes, A., Carlotto, V., López, S., 2010. Geodynamic evolution of the early Paleozoic Western Gondwana margin 14°–17°S reflected by the detritus of the Devonian and Ordovician basins of southern Peru and northern Bolivia. Gondwana Res. 18, 370–384.
Reiners, P.W., Thomson, S.N., Vernon, A., Willett, S.D., Zattin, M., Einhorn, J., Gehrels, G., Quade, J., Pearson, D., Murray, K.E., 2015. Low-temperature thermochronologic trends across the central Andes, 21°S–28°S. In: Geological Society of America Memoirs, vol. 212, pp. 215–249.
Rivadeneyra-Vera, C., Bianchi, M., Assumpção, M., Cedraz, V., Julià, J., Rodríguez, M., Sánchez, L., Sánchez, G., Lopez-Murua, L., Fernandez, G., 2019. An updated crustal thickness map of central South America based on receiver function measurements in the region of the Chaco, Pantanal, and Paraná Basins, southwestern Brazil. J. Geophys. Res., Solid Earth 124, 8491–8505.
Rochat, P., Hérail, G., Baby, P., Mascle, G., Aranibar, O., 1998. Analyse géométrique et modèle tectonosédimentaire de l'Altiplano Nord-Bolivien. C. R. Acad. Sci., Sér. IIA Earth Planet. Sci., vol. 327, pp. 769–775.
Roperch, P., Fornari, M., Hérail, G., Parraguez, G.V., 2000. Tectonic rotations within the Bolivian Altiplano: implications for the geodynamic evolution of the central Andes during the late Tertiary. J. Geophys. Res., Solid Earth 105, 795–820.
Roperch, P., Sempere, T., Macedo, O., Arriagada, C., Fornari, M., Tapia, C., Garcia, M., Laj, C., 2006. Counterclockwise rotation of late Eocene-Oligocene fore-arc deposits in southern Peru and its significance for oroclinal bending in the central Andes. Tectonics 25.
Roperch, P., Carlotto, V., Ruffet, G., Fornari, M., 2011. Tectonic rotations and transcurrent deformation south of the Abancay deflection in the Andes of southern Peru. Tectonics 30.

Rousse, S., Gilder, S., Fornari, M., Sempere, T., 2005. Insight into the Neogene tectonic history of the northern Bolivian Orocline from new paleomagnetic and geochronologic data. Tectonics 24.

Rudolph, K.W., Devlin, W.J., Carabaugh, J.P., 2015. Upper Cretaceous sequence stratigraphy of the Rock Springs Uplift, Wyoming. Mt. Geol. 52, 13–157.

Ruiz, G.M.H., Carlotto, V., v. Heiningen, P.V., Andriessen, P.A.M., Lisker, F., Ventura, B., Glasmacher, U.A., 2009. Steady-state exhumation pattern in the Central Andes – SE Peru. In: Thermochronological Methods: From Palaeotemperature Constraints to Landscape Evolution Models. Geological Society of London, pp. 307–316.

Runyon, B., Saylor, J.E., Horton, B.K., Reynolds, J.H., Hampton, B., 2021. Basin evolution in response to flat-slab subduction in the Altiplano. J. Geol. Soc.

Sandeman, H.A., Clark, A.H., Farrar, E., 1995. An integrated tectono-magmatic model for the evolution of the southern Peruvian Andes (13-20S) since 55 Ma. Int. Geol. Rev. 37, 1039–1073.

Saylor, J.E., Horton, B.K., 2014. Nonuniform surface uplift of the Andean plateau revealed by deuterium isotopes in Miocene volcanic glass from southern Peru. Earth Planet. Sci. Lett. 387, 120–131.

Saylor, J.E., Rudolph, K.W., Sundell, K.E., van Wijk, J.W., 2020. Laramide orogenesis driven by Late Cretaceous weakening of the North American lithosphere. J. Geophys. Res., Solid Earth 125, e2020JB019570.

Saylor, J.E., Sundell, K.E., 2021. Tracking Proterozoic–Triassic sediment routing to western Laurentia via bivariate non-negative matrix factorization of detrital provenance data. J. Geol. Soc.

Scheuber, E., Mertmann, D., Ege, H., Silva-Gonzalez, P., Heubeck, C., Reutter, K.-J., Jacobshagen, V., 2006. Exhumation and basin development related to formation of the central Andean plateau, 21°S. In: Oncken, O., Chong, G., Franz, G., Giese, P., Gotze, H.-J., Ramos, V.A., Strecker, M.R., Wigger, P. (Eds.), The Andes: Active Subduction Orogeny. Springer-Verlag, Berlin, pp. 285–301.

Schildgen, T.F., Hodges, K.V., Whipple, K.X., Reiners, P.W., Pringle, M.S., 2007. Uplift of the western margin of the Andean plateau revealed from canyon incision history, southern Peru. Geology 35, 523–526.

Schildgen, T.F., Ehlers, T.A., Whipp, D.M., van Soest, M.C., Whipple, K.X., Hodges, K.V., 2009a. Quantifying canyon incision and Andean Plateau surface uplift, southwest Peru: a thermochronometer and numerical modeling approach. J. Geophys. Res., Earth Surf. 114.

Schildgen, T.F., Hodges, K.V., Whipple, K.X., Pringle, M.S., van Soest, M., Cornell, K., 2009b. Late Cenozoic structural and tectonic development of the western margin of the central Andean Plateau in southwest Peru. Tectonics 28.

Sempere, T., 1995. Phanerozoic evolution of Bolivia and adjacent regions.

Sempere, T., Butler, R.F., Richards, D.R., Marshall, L.G., Sharp, W., Swisher, C.C., 1997. Stratigraphy and chronology of upper Cretaceous lower Paleogene strata in Bolivia and northwest Argentina. Geol. Soc. Am. Bull. 109, 709–727.

Smith, T.M., Saylor, J.E., Leary, R.J., Lapen, T.J., 2023. Large detrital zircon data set investigation and provenance mapping: local versus regional and continental sediment sources before, during, and after Ancestral Rocky Mountain deformation. Geol. Soc. Am. Bull. https://doi.org/10.1130/B36285.1. Accepted.

Spikings, R., Reitsma, M.J., Boekhout, F., Mišković, A., Ulianov, A., Chiaradia, M., Gerdes, A., Schaltegger, U., 2016. Characterisation of Triassic rifting in Peru and implications for the early disassembly of western Pangaea. Gondwana Res. 35, 124–143.

Strecker, M.R., Hilley, G.E., Bookhagen, B., Sobel, E.R., 2011. Structural, geomorphic, and depositional characteristics of contiguous and broken foreland basins: examples from the eastern flanks of the Central Andes in Bolivia and NW Argentina. In: Tectonics of Sedimentary Basins. John Wiley & Sons, Ltd, pp. 508–521.

Sundell, K.E., 2017. Cenozoic Surface Uplift and Basin Formation in the Peruvian Central Andes. Earth and Atmospheric Sciences. University of Houston, Houston, p. 256.

Sundell, K.E., Saylor, J.E., 2017. Unmixing detrital geochronology age distributions. Geochem. Geophys. Geosyst. 18.

Sundell, K.E., Saylor, J.E., Lapen, T.J., Styron, R.H., Villareal, D., Usnayo, P., Cardenas, J., 2018. Peruvian Altiplano stratigraphy highlights along-strike variability in foreland basin evolution of the Cenozoic central Andes. Tectonics 37, 1876–1904.

Sundell, K.E., Saylor, J.E., Lapen, T.J., Horton, B.K., 2019. Implications of variable late Cenozoic surface uplift across the Peruvian central Andes. Sci. Rep. 9, 4877.

Trumbull, R.B., Riller, U., Oncken, O., Scheuber, E., Munier, K., Hongn, F., 2006. The time-space distribution of Cenozoic volcanism in the South-Central Andes: a new data compilation and some tectonic implications. In: The Andes. Springer, pp. 29–43.

van Hunen, J., van den Berg, A.P., Vlaar, N.J., 2004. Various mechanisms to induce present-day shallow flat subduction and implications for the younger Earth: a numerical parameter study. Phys. Earth Planet. Inter. 146, 179–194.

Vermeesch, P., 2021. Maximum depositional age estimation revisited. Geosci. Front. 12, 843–850.

Vicente, J.-C., 1990. Early Late Cretaceous overthrusting in the Western Cordillera of southern Peru. In: Ericksen, G.E., Canas Pinochet, M.T., Reinemund, J.A. (Eds.), Geology of the Andes and Its Relation to Hydrocarbon and Mineral Resources. In: Circum-Pacific Council for Energy and Mineral Resources Earth Science Series, pp. 91–117.

Ward, K.M., Zandt, G., Beck, S.L., Wagner, L.S., Tavera, H., 2016. Lithospheric structure beneath the northern Central Andean Plateau from the joint inversion of ambient noise and earthquake-generated surface waves. J. Geophys. Res., Solid Earth 121, 8217–8238.

Wipf, M., Zeilinger, G., Seward, D., Schlunegger, F., 2008. Focused subaerial erosion during ridge subduction: impact on the geomorphology in south-central Peru. Terra Nova 20, 1–10.

Wotzlaw, J.F., Decou, A., von Eynatten, H., Wörner, G., Frei, D., 2011. Jurassic to Palaeogene tectono-magmatic evolution of northern Chile and adjacent Bolivia from detrital zircon U-Pb geochronology and heavy mineral provenance. Terra Nova 23, 399–406.